

ORIGINAL ARTICLE

Specific detection and deletion of the sigma-1 receptor widely expressed in neurons and glial cells in vivo

Qing Liu¹  | Qilin Guo¹  | Li-Pao Fang¹  | Honghong Yao² | Anja Scheller¹  | Frank Kirchhoff¹  | Wenhui Huang¹ 

¹Molecular Physiology, CIPMM, University of Saarland, Homburg, Germany

²Department of Pharmacology, School of Medicine, Southeast University, Nanjing, China

Correspondence

Wenhui Huang and Frank Kirchhoff, Molecular Physiology, Center for Integrative Physiology and Molecular Medicine (CIPMM), University of Saarland, 66421 Homburg, Germany.
 Email: wenhui.huang@uks.eu; frank.kirchhoff@uks.eu

Funding information

Bundesministerium für Bildung und Forschung, Grant/Award Number: EraNet-Neuron BrE; Fritz Thyssen Foundation, Grant/Award Number: 10.21.1.021MN; National Natural Science Foundation of China, Grant/Award Number: 81761138048; European Commission, Grant/Award Number: EC-H2020 FET ProAct Neurofibres; Deutsche Forschungsgemeinschaft, Grant/Award Number: HU 2614/1-1 (project ID: 462650276), KI 503/14, SFB894 A12 and SPP 1757

Abstract

The chaperon protein sigma-1 receptor (S1R) has been discovered over 40 years ago. Recent pharmacological studies using S1R exogenous ligands demonstrated a promising therapeutical potential of targeting the S1R in several neurological disorders. Although intensive in vitro studies have revealed S1Rs are mainly residing at the membrane of the endoplasmic reticulum (ER), the cell-specific in vivo expression pattern of S1Rs is still unclear, mainly because of the lack of a reliable detection method which also prevented a comprehensive functional analysis. Here, first, we identified a highly specific antibody using S1R knockout (KO) mice and established an immunohistochemical protocol involving a 1% sodium dodecyl sulphate (SDS) antigen retrieval step. Second, we characterized the S1R expression in the mouse brain and can demonstrate that the S1R is widely expressed: in principal neurons, interneurons and all glial cell types. In addition, unlike reported in previous studies, we showed that the S1R expression in astrocytes is not colocalized with the astrocytic cytoskeleton protein GFAP. Thus, our results raise concerns over previously reported S1R properties. Finally, we generated a Cre-dependent S1R conditional KO mouse (S1R flox) to study cell-type-specific functions of the S1R. As a proof of concept, we successfully ablated S1R expressions in neurons or microglia employing neuronal and microglial Cre-expressing mice, respectively. In summary, we provide powerful tools to cell-specifically detect, delete and functionally characterize S1R in vivo.

1 | INTRODUCTION

The sigma-1 receptor (S1R) is a chaperon protein primarily residing at mitochondria-associated membranes (MAM) of the endoplasmic

reticulum (ER) with a single membrane-spanning domain, which is considered as a pluripotent modulator involved in many aspects of cellular functions (Lee et al., 2020; Su, Su, Nakamura, & Tsai, 2016; Zhemkov et al., 2021). Previous studies by immunohistochemistry

Abbreviations: AR, antigen retrieval; Ab, antibody; calb, calbindin; CNS, central nervous system; ctx, cortex; cc, corpus callosum; Cpu, caudate putamen; ER, endoplasmic reticulum; EtOH, ethanol; GFAP, glial fibrillary acidic protein; GS, glutamine synthetase; GM, grey matter; HA, human influenza haemagglutinin; hip, hippocampus; HRP, horse-radish peroxidase; KO, knockout; MAM, mitochondria-associated membranes; MACS, magnetic-activated cell sorting; MFI, mean fluorescence intensity; NC, nitrocellulose; NEX, neuronal helix-loop-helix protein-1; OL, oligodendrocyte; OPC, oligodendrocyte precursor cell; PV, parvalbumin; P α , PDGFR α , platelet-derived growth factor receptor α ; qPCR, quantitative real-time PCR; ROI, region of interest; RT, room temperature; SDS, sodium dodecyl sulphate; S1R, sigma-1 receptor; sc, spinal cord; Sst, somatostatin; SWI, stab wound injuries; WT, wild type; WM, white matter.

This is an open access article under the terms of the [Creative Commons Attribution](https://creativecommons.org/licenses/by/4.0/) License, which permits use, distribution and reproduction in any medium, provided the original work is properly cited.

© 2022 The Authors. *Journal of Neurochemistry* published by John Wiley & Sons Ltd on behalf of International Society for Neurochemistry.



(IHC) and mRNA expression profiling experiments suggested that S1Rs are highly expressed in the central nervous system (CNS) and can also be detected in other organs such as liver, kidney and muscles (Couly et al., 2022; Su et al., 2016; Zhang et al., 2014). However, it is still hard to conclude the cellular expression patterns of S1R in the CNS because of seemingly paradoxical results obtained by IHC. For instance, using a custom-made antibody Alonso et al. detected S1Rs only in neurons in the brain and spinal cord, while Palacios et al., using an independently custom-made antibody could observe S1R expression also in oligodendrocytes (OLs) (Alonso et al., 2000; Palacios et al., 2003), and Ruscher et al., using a commercial antibody observed S1R immunoreactivity co-localized with the cytoskeleton indicated by glial fibrillary acidic protein (GFAP) as well as with the galactocerebroside-enriched membrane microdomains of reactive astrocytes in the peri-infarct area of rat brains after cerebral stroke (Ruscher et al., 2011). Of note, it is not clear whether the specificity of the antibodies used in the aforementioned studies was tested by S1R KO mice/cell lines as rigorous controls. To date, only one custom-made antibody against S1R (termed Ab^{Ruoho}) generated by Arnold Ruoho's group was validated by S1R KO mice, showing high specificity for IHC in the brain and spinal cord (though it did not work well for immunoblot) (Mavlyutov et al., 2016; Mavlyutov, Epstein, Andersen, Ziskind-Conhaim, & Ruoho, 2010; Nakamura et al., 2019). However, in these studies, the fine structures of Ab^{Ruoho} stained cells in brain slices were not displayed with high magnification, neither were co-immunostainings combined for different cell type markers with Ab^{Ruoho} performed. Therefore, it is hard to verify the detailed expression pattern of S1Rs in neurons and glial cells in vivo.

Neurons and glial cells interact with each other to orchestrate diverse CNS functions. Previous studies using constitutive S1R KO mice suggest S1Rs are involved in the maintenance of cognitive, psychiatric and motor functions, particularly with ageing (Couly et al., 2022). Moreover, the S1R is considered as an enigmatic therapeutic target for various neurological disorders (e.g. Alzheimer's disease, Parkinson's disease, amyotrophic lateral sclerosis, multiple sclerosis, etc.) upon activation by its exogenous ligands including agonists and antagonists (Sałaciak & Pytka, 2022; Schmidt & Kruse, 2019). However, the contribution of cell-type-specific S1Rs to modulate the neural network activity under physiological and pathological conditions as well as upon activation is still not well understood, which could be addressed by inducing S1R deletion or overexpression in targeted cells in vivo.

In the current work, we prepared tissue lysates of brains and spinal cords from WT and S1R KO mice to screen six commercial antibodies against the S1R for their immunospecificity by immunoblot. We obtained one rabbit monoclonal antibody (#61994, Cell Signaling) displaying very high specificity for S1R by Western blot analysis. We further revealed that after the antigen retrieval (AR) using 1% sodium dodecyl sulphate (SDS), this antibody demonstrated highly specific immunolabelling of S1Rs in situ in the CNS. Combining immunostaining for different cell type markers, we identified that S1Rs were widely expressed in the CNS, that is, in principal

neurons, interneurons, astrocytes, oligodendrocyte precursor cells (OPCs), OLs and microglia. In addition, we found that unlike previous reports (Francardo et al., 2014; Ruscher et al., 2011), S1R expression in astrocytes was not correlated with the GFAP-labelled cytoskeleton, neither in healthy brain slices nor after acute brain injuries. Second, we generated a S1R flox mouse with exons 1–3 of *Sigmar1* (gene name of S1R, also called *Opr1*) flanked by two loxP sites. By cross-breeding this S1R flox mouse with two Cre-driver mouse lines targeting neurons and microglia, respectively, we were able to show the specific deletion of S1Rs in targeted cells in vivo. Taken together, we introduce a reliable protocol to detect S1Rs, which are broadly expressed in the CNS, by immunoblotting and IHC. We also provide a newly generated S1R flox mouse for cell-type-specific ablation of S1Rs in vivo. In the future, these tools will facilitate the functional analysis of S1Rs in vivo.

2 | MATERIALS AND METHODS

2.1 | Animals

All mice (C57BL/6 background) used in this study were maintained at the animal facility of the CIPMM in a temperature- ($22^{\circ}\text{C} \pm 2^{\circ}\text{C}$) and humidity-controlled facility with a 12-h light/dark cycle. Animal husbandry and procedures were performed at the animal facility of CIPMM, University of Saarland according to European and German guidelines for the welfare of experimental animals. Animal experiments were approved by the Saarland state's 'Landesamt für Gesundheit und Verbraucherschutz' in Saarbrücken/Germany (animal license number: 34/2016, 36/2016, 03/2021 and 08/2021). The study was not preregistered. Each mouse was given an animal ID in an animal administrative system (PyRAT, Python-based Relational Animal Tracking, Scionics Computer Innovation, Dresden). In detail, on weaning days mice in each litter were marked by ear punches to acquire IDs by animal caretakers of the CIPMM. Assignment of animals with different IDs at different ages was arbitrarily performed to study groups as indicated in figures. Pre-determination of the sample size, and blinding procedure were not performed in the study. A total of 69 mice were used in this exploratory study, and initial number of animals used per group was three. No exclusion criteria were pre-determined and no animals were excluded during experiments.

For antibody testing, 4- to 8-week-old mice of either sex were used in this study. *Sigmar1* global knockout (S1R KO) mice were generated by GemPharmatech (Nanjing, China) by deleting the entire encoding region (~10359 bp) of *Sigmar1*. TgN(Thy1-HcRed) (Hirrlinger et al., 2005) mice in which excitatory neurons express HcRed fluorescent proteins under the Thy1 promoter were used to identify the S1R expression in excitatory neurons.

RiboTag mice (Rlp22^{HA}) (Sanz et al., 2009) were introduced to immunoprecipitate HA (human influenza haemagglutinin)-tagged ribosome-associated translated mRNA in targeted glial cells upon breeding with different glia-specific Cre-driver mice ($n = 3$ mice per mouse line). Specifically, GLAST-CreERT2 mice for astrocytes (Mori

et al., 2006), CX3CR1-CreERT2 mice for microglia (Yona et al., 2013) and NG2-CreERT2 mice for OPCs (Huang et al., 2014) were used.

The *Sigmar1* flox (*S1R^{fl/fl}*) mouse line was generated through the 'Dalmatian Mouse Action' of GemPharmatech (Nanjing, China). CRISPR/Cas9 technology was used to modify the *Sigmar1* gene (*Opr1*). Briefly, single guide RNA (sgRNA) was transcribed in vitro, and the donor vector containing exons 1–3 of *Sigmar1* flanked by two loxP sites was constructed. Cas9, sgRNA and the donor vector were microinjected into the fertilized eggs of C57BL/6J mice. sgRNA directed Cas9 endonuclease cleavage at about 6 kb upstream of exon1 and downstream of 3'UTR and create a double-strand break (DSB). The following primer sequences were used for genotyping PCR (forward: 5'-AAG CAG AAG AGC AGC TAG TGC TG-3', reverse: 5'-TGA GAC AGG GTT TCT CTG TAT AGC C-3').

To obtain cell-type-specific *S1R* knockout mice, *S1R^{fl/fl}* mice were crossed to NEX-Cre mice (NEX for neuronal helix–loop–helix protein-1, also called NeuroD6) (Goebbels et al., 2006) to induce the specific knockout of *S1R*s in principal neurons within the dorsal telencephalon and hippocampus or crossed to CX3CR1-CreERT2 mice (Yona et al., 2013) to induce the knockout of *S1R*s in microglia upon tamoxifen administration. Both conditional *S1R* knockout mice showed normal fertility and normal brain morphology, and do not show overt changes in body size and behaviour.

2.2 | Tamoxifen induction

Tamoxifen (cat. no.: CC99648, Carbobution) was dissolved in Miglyol (cat. no.: 3274, Caesar & Loretz, Hilden) at a concentration of 10 mg/ml. All mice crossed with CreERT2-driver mouse lines were injected intraperitoneally with tamoxifen (100 mg/kg of bodyweight) for five consecutive days at the age of 4 weeks.

2.3 | Stab wound injury (SWI) model

Adult mice (10 weeks old) were used for stab wound injuries (SWI) as described before with some modifications (Huang, Bai, Meyer, & Scheller, 2020). Briefly, 1 h before the surgery, animals were given carprofen (5 mg/kg bodyweight) subcutaneously. Subsequently, under 1.5% isoflurane anaesthesia, animals were fixed in a stereotaxic frame with a heat plate. After sterile cleaning and skin incision, a 2 mm cranial groove was drilled in the right neocortex at Bregma from 0.5–2.5 mm, lateral 1.5 mm. A sterile razor blade (2 mm width) was inserted vertically into brain parenchyma (1 mm deep) parallel with the middle line. The lesion was cleaned and closed with sutures. Animals were post-surgically subcutaneous injected carprofen (5 mg/kg bodyweight) per day for the next 2 days for pain relief. After 3 and 7 days post injury (3 dpi, 7 dpi), mice ($n = 3$ per time point) were deeply anesthetized and perfused with 4% paraformaldehyde (PFA) dissolved in 0.1 M phosphate buffer (PB, PH 7.4). Coronal sections (35 μ m) were collected and used for immunostaining.

2.4 | Magnetic-associated cell sorting (MACS) of glial cells

MACS was performed according to the manufacturer's instruction (Miltenyi Biotec) with some modifications as shown previously (Fang et al., 2022). In brief, 4-week-old mice were perfused with cold Hank's balanced salt solution without Ca^{2+} and Mg^{2+} (HBSS, cat. no.: H6648, Gibco) and cortices were dissected in ice-cold HBSS. After the removal of debris (cat. no.: 130-107-677, Miltenyi Biotec), cells were resuspended with 1 ml 're-expression medium' containing NeuroBrew-21 (1:50 in MACS neuro Medium) (cat. no.: 130-093-566 and 130-093-570, Miltenyi Biotec) and 200 mL-glutamine (1:100, cat. no.: G7513, Sigma-Aldrich) at 37°C for 30 min.

For OPC sorting, cells were incubated with Fc-receptor blocker (provided with the CD140 microbeads kit) for 10 min at 4°C, followed by a 15 min incubation with 10 μ l microbeads mixture containing antibodies directed against CD140 (cat. no.: 130-101-502, Miltenyi Biotec), NG2 (cat. no.: 130-097-170, Miltenyi Biotec) and O4 (cat. no.: 130-096-670, Miltenyi Biotec) in 1:1:1 at 4°C.

For sorting of astrocytes, microbeads containing antibodies directed against ACSA-2 (cat. no.: 130-097-678, Miltenyi Biotec) were used.

For microglia sorting, microbeads containing antibodies directed against CD11b (cat. no.: 130-093-634, Miltenyi Biotec) were used.

2.5 | Western blot analysis

After anaesthesia with 250 mg/kg ketamine and 50 mg/kg xylazine, mice were transcardially perfused with ice-cold PBS. The dorsal region of the cortex was dissected from coronal brain slices (1 mm). Segments from the cervical spinal cord segment were collected. Specimens were stored at -80°C until tested. RIPA lysis buffer (cat. no.: 89900, Thermo Fisher Scientific) containing 1x protease inhibitor cocktail (cat. no.: 05892970001, Roche) was used to extract protein. Protein concentration was measured using the Bicinchoninic Acid (BCA) assay kit (cat. no.: 23225, Thermo Fisher Scientific). After adding 1x protein loading buffer (cat. no.: 42526.01, SERVA) containing 5% β -mercaptoethanol (cat. no.: M6250, Sigma-Aldrich), protein samples were denatured 5 min at 95°C. Equal amounts of lysates (10–30 μ g) of each mouse were separated by 10% SDS-polyacrylamide gel electrophoresis (PAGE, cat. no.: 43289.01, SERVA) and transferred onto nitrocellulose (NC) membranes (cat. no.: QP0907015, neoLab). Homogeneous protein-transfer onto NC membranes was evaluated by Ponceau S staining. After blocking with 5% non-fat milk powder (cat. no.: A0830, 0500, PanReac AppliChem) in 1x PBS for 1 h at room temperature (RT, 20–22°C), NC membranes were incubated with primary antibodies at 4°C overnight (Table 1) in TBST solution (Tris-base buffer with 0.1% Tween-20). The next day, membranes were washed three times with TBST and incubated with corresponding horseradish peroxidase (HRP) conjugated secondary antibodies (Table 2) in TBST for 1 h at RT. For detecting different proteins on the same NC membrane, the

TABLE 1 Primary antibodies used for Western blot and immunohistochemistry

Antigen	Host species	Antibody type	Source	Catalog no.	Dilution
Sigma-1 receptor (D4J2E)	Rabbit	Monoclonal	Cell Signaling	#61994	WB: 1:1000, IHC: 1:500
Sigma-1 receptor (D7L1M)	Rabbit	Monoclonal	Cell Signaling	#74807	WB: 1:1000, IHC: 1:500
Sigma-1 receptor (B-5)	Mouse	Monoclonal	Santa Cruz	sc-137075	WB: 1:500, IHC: 1:500
Sigma-1 receptor	Rabbit	Polyclonal	Invitrogen	#42-3300	WB: 1:500, IHC: 1:500
Sigma-1 receptor C-terminal	Rabbit	Polyclonal	Abcam	Ab53852	WB: 1:500, IHC: 1:500
Sigma-1 receptor	Rabbit	Polyclonal	Proteintech	15 168-1-AP	WB: 1:500, IHC: 1:500
CD11b	Rabbit	Monoclonal	Abcam	Ab133357	WB: 1:1000, IHC: 1:500
GFAP	Rabbit	Polyclonal	Dako	Z 0334	WB: 1:1000, IHC: 1:500
GAPDH	Mouse	Monoclonal	Sigma-Aldrich	G8795	WB: 1:1000, IHC: 1:500
α -Tubulin	Mouse	Monoclonal	Sigma-Aldrich	T6074	WB: 1:1000, IHC: 1:500
GS	Mouse	Monoclonal	BD	610 518	IHC: 1:500
GFAP	Goat	Polyclonal	Abcam	Ab53554	IHC: 1:500
PDGFR α	Goat	Polyclonal	R&D Systems	AF1042	IHC: 1:500
APC (Ab-7) clone CC-1	Mouse	Monoclonal	Calbiochem	OP80	IHC: 1:200
Iba1	Goat	Polyclonal	Abcam	ab5076	IHC: 1:500
S100 beta SH-B1	Mouse	Monoclonal	Abcam	ab66028	IHC: 1:500
Calbindin-D28K	Mouse	Monoclonal	Sigma-Aldrich	C9848	IHC: 1:500
NeuN Clone A60	Mouse	Monoclonal	Millipore	MAB377	IHC: 1:500
MBP Myelin Basic Protein (MBP)	Mouse	Monoclonal	Biolegend	SM199	IHC: 1:500
a-Actinin (Sarcomeric) clone EA-53	Mouse	Monoclonal	Sigma-Aldrich	A7811	IHC: 1:500
SERCA2	Mouse	Monoclonal	Sigma-Aldrich	S1439	IHC: 1:500

Correction added on 8th October 2022, after first online publication: the antigen names in rows 2 and 5 of Table 1 have been corrected in this version

TABLE 2 Secondary antibodies and nuclear stains used for Western blot and immunohistochemistry

Antibody	Source	Catalog no.	Dilution
goat anti-rabbit IgG HRP	Dianova	111-035-045	WB: 1: 5000
goat anti-mouse IgG HRP	Sigma-Aldrich	A9044	WB: 1: 10000
Alexa Fluor 488 donkey anti-mouse	Invitrogen	A21202	IHC: 1: 1000
Alexa Fluor 488 donkey anti-goat	Invitrogen	A11055	IHC: 1: 1000
Alexa Fluor 546 donkey anti-mouse	Invitrogen	A10036	IHC: 1: 1000
Alexa Fluor 647 donkey anti-rabbit	Invitrogen	A31573	IHC: 1: 1000
DAPI (stain for nuclei)	BioChemica	A10010010	IHC: 0.025 μ g/ml

previous antibodies were stripped off by stripping buffer (cat.no.: 21059, Thermo Fisher Scientific) for 20min and then incubated with other primary antibodies.

For MACS-purified cells, 40 μ l RIPA lysis buffer (cat. no.: 89900, Thermo Fisher Scientific) and the equal amount of 1x loading buffer with 5% β -mercaptoethanol were added per sample. After denaturation for 5 min at 95°C, 10 μ l of each protein sample was separated by SDS-PAGE and assessed by Western blot as described above. All primary antibodies are listed in Table 1 and secondary antibodies in Table 2, respectively.

The immunoblots were processed using enhanced chemiluminescence (ECL) reagent (cat. no.: 541015, Biozym) and ChemiDoc Imaging System (BioRad). The immunoblot intensity was quantified with ImageJ software (ImageJ 1.53q, NIH).

2.6 | Immunohistochemistry

After anaesthesia (250 mg/kg ketamine and 50 mg/kg xylazine, i.p.), mice were transcardially perfused with 5 ml PBS and followed with 15ml 4% PFA. Dissected brains were post-fixed in 4% PFA at 4°C overnight. Then, coronal brain sections or transverse spinal sections were prepared by vibratome (VT1000S, Leica). The regular free-floating immunostaining was performed as previously described (Huang et al., 2020). Two new protocols with AR were established for S1R staining with the antibody #61994:

AR^{SDS} protocol for immunostaining of S1Rs in the brain: brain slices were pre-treated with 1% SDS (cat. no.: CN30.1, Roth) in 1x PBS for 10 min at RT (20-22°C) for AR (Brown et al., 1996). After three times washing with 1x PBS, the blocking buffer (1x Fish



Gelatin Blocking Agent (cat. no.: 22010, BioTium), 0.5% Triton x-100 (cat. no.: A1388, BioChemica) in PBS) was added to slices and incubated for 60 min at RT (20–22°C) to decrease background signal. All primary antibodies were diluted in blocking buffer.

AR^{EtOH-SDS} protocol for S1R immunostaining in the spinal cord: spinal slices were incubated with 100% ethanol (EtOH) at 4°C overnight with gentle shake for delipidation. After washing with 1x PBS, 1% SDS pre-treatment was performed as described in AR^{SDS} protocol above.

To co-immunostain S1R with the ER marker SERCA2, blocking buffer containing 0.5% NP-40 (cat. no.: 74385, Sigma-Aldrich) instead of Triton X-100 was used for SERCA2 staining prior to S1R staining. After incubation with the secondary antibody against SERCA2 antibody, slices were fixed with 2% PFA for 30 min, followed by immunostaining of S1Rs with the AR^{SDS} protocol.

Brain and spinal cord slices were incubated at 4°C overnight with primary antibodies at appropriate dilutions as shown in Table 1. After washing with 1x PBS, sections were incubated with corresponding secondary antibodies (Table 2) for 2 h at RT (20–22°C). DAPI was used for nuclear staining. After washing three times with 1x PBS, slices were mounted with Immu-Mount (cat. no.: 9990402, Thermo) (Figure 2a).

2.7 | Ribosome immunoprecipitation (IP)

After perfusion with ice-cold HBSS, cortical samples were dissected from mouse brain and stored at –80°C until use. Tissues were homogenized in ice-cold lysis buffer (50 mM Tris, pH 7.4, 100 mM KCl, 12 mM MgCl₂, 1% NP-40, 1 mM DTT, 1x protease inhibitor, 200 units/ml RNasin (cat. no.: N2515, Promega) and 0.1 mg/ml cycloheximide (cat. no.: C7698, Sigma-Aldrich) in RNase-free deionized H₂O) 10% w/v with homogenizer (Precellys 24, PeQlab). Homogenates were centrifuged at 10000g at 4°C for 10 min to remove cell debris. Supernatants were collected, from which 50 µl were removed for input analysis. Anti-HA-tag Ab (1:100, cat. no.: MMS-101P, Covance) was added to the supernatant and slowly rotated at 4°C. Protein G-Dynabeads (cat. no.: 01205884, Thermo Fisher Scientific) were equilibrated with lysis buffer by washing three times. After 4 h of incubation with HA-tag Ab, 100 µl pre-equilibrated beads were added to each sample and incubated overnight at 4°C. After 10–12 h, samples were washed with high-salt buffer (50 mM Tris, 300 mM KCl, 12 mM MgCl₂, 1% NP-40, 1 mM DTT, 1x protease inhibitor, 100 units/ml RNasin and 0.1 mg/ml cycloheximide in RNase-free deionized H₂O) three

times for 5 min at 4°C. At the end of the washing, beads were magnetized and 150 µl RA1 lysis buffer from NucleoSpin RNA Plus XS Kit (cat. no.: 40990.50, Macherey-Nagel) was added to the beads. RNA was extracted followed with manufacturer's instructions (NucleoSpin RNA Plus XS, Macherey-Nagel).

2.8 | Quantitative real-time PCR (qPCR)

RNA concentration was determined using NanoDrop from IP and input RNA. One hundred micrograms of RNA was used to synthesize first-strand complementary DNA (cDNA) using Omniscript kit (cat. no.: 205113, QIA-GEN). qPCR was performed with EvaGreen (cat. no.: 27490, Axon) in a CFX96 Real-Time System (BioRad). The standard two-step program was used: 94°C for 10 min, then 40 cycles at 94°C for 15 s, 60°C for 1 min. The expression of *Sigmar1*, *Gfap*, *Itgam* and *Pdgfra* was quantified. For primer see Table 3. Relative expression of targeted genes was determined using the $\Delta\Delta C_t$ method with normalization to β -actin (*Actb*) expression.

2.9 | Image acquisition and quantification

Images were acquired using an epifluorescence microscope system AxioScan.Z1 (Zeiss), with a Plan-Apochromat 20x/0.8 M27 objective and a Zeiss confocal microscope system LSM 880 with Plan-Apochromat 40x/1.3 Oil DIC UV-IR M27 objective (Zeiss).

For each immunostaining, two coronal brain sections per mouse were collected randomly at the hippocampal level. Epifluorescence AxionScan images were used for quantification of S1R expression in NeuN⁺ cells using ZEN 3.1 (blue edition) software (Figure 3a,g). For quantification of S1R expression in neurons and glial cells (Figures 3h–j; Figure 4e,f; 5e,f; 6e,f; 7e,f) as well as in NeuN⁺ cells in NEX-Cre x S1R^{fl/fl} mice (Figure 10d,e), non-overlapping confocal image stacks were arbitrarily taken from areas of the six cortical layers, two different areas from corpus callosum, two different areas from striatum, one area from thalamus and hypothalamus. To quantify S1R expression levels in individual neurons and glial cells (Figure S10), non-overlapping confocal image stacks were arbitrarily taken from deep cortical layers (L5 and 6) from two slices per mouse ($n = 3$ mice) with the same imaging settings (laser power: 2%, gain: 0.9). For analyzing the deletion of S1R in microglia in CX3CR1-CreERT2 x S1R^{fl/fl} mice, non-overlapping confocal images were arbitrarily taken from three areas over the dorsal cortex. Cell counting and mean fluorescence

Gene	Forward primer (5'-3')	Reverse primer (5'-3')
<i>Sigmar1</i>	CTGGGCACTCAAACCTTCGTC	CTCCACGATCAGCCGAGAGA
<i>Gfap</i>	GCCACCAGTAACATGCAAGA	CAGCGTCTGTGAGGTCTG
<i>Itgam</i>	CAATAGCCAGCCTCAGTGC	GAGCCCAGGGGAGAAGTG
<i>Pdgfra</i>	ACCTCCACCAAGGTCTTTCT	CTTCACTCTCCCAACGCAT
<i>Actb</i>	CTTCTCCCTGGAGAAGAGC	ATGCCACAGGATCCATACC

TABLE 3 Primer sequences used for the qPCR analysis

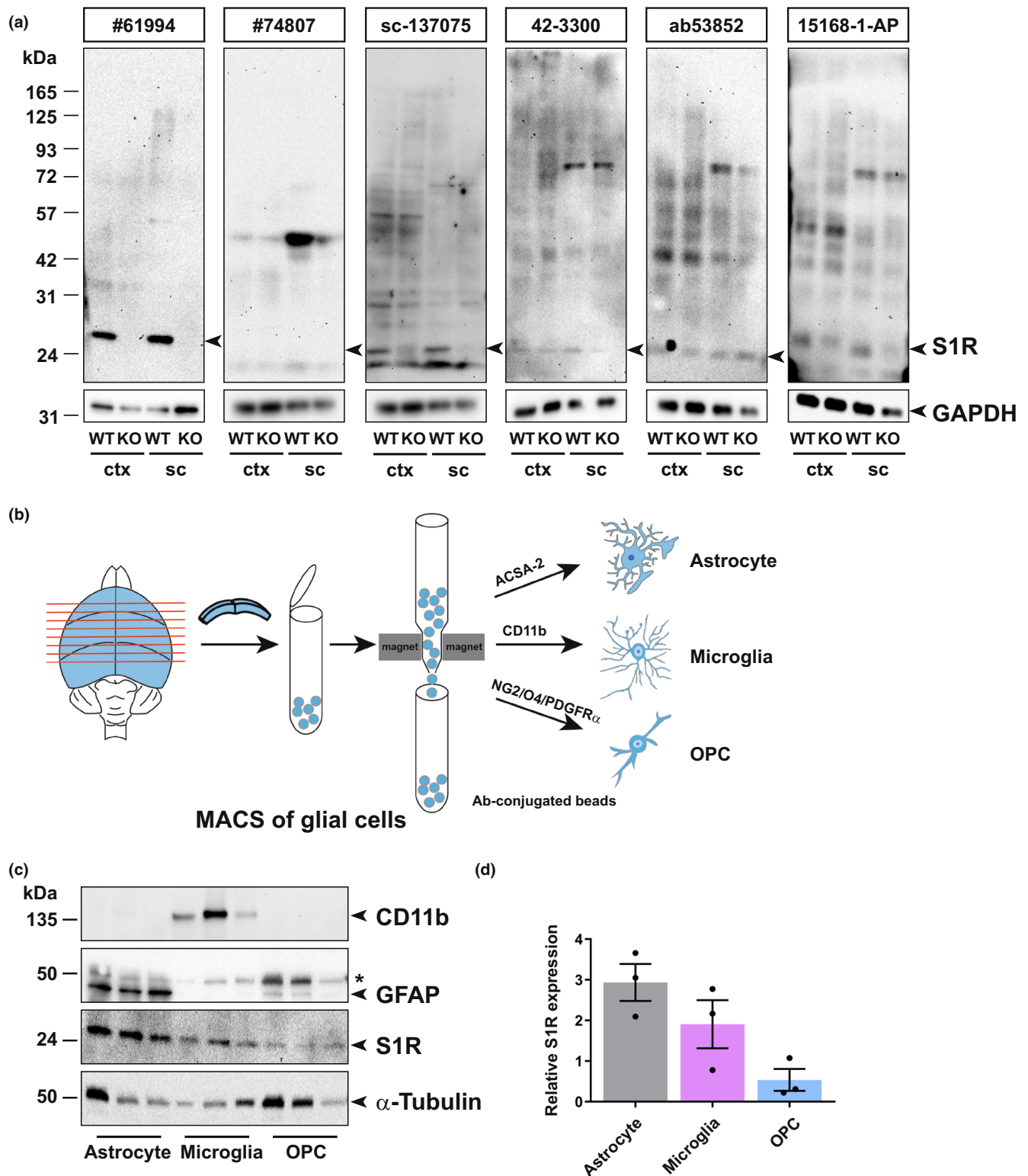


FIGURE 1 Detection of S1Rs in the CNS by immunoblot. (a) Full-length scan of the S1R immunoblot of protein lysates from cortex (ctx) and spinal cord (sc) tissue of WT and S1R KO mice. S1R antibodies (Abs) from Cell Signaling (#61994 and #74807), Santa Cruz (sc-137075), Invitrogen (42-3300), Abcam (ab53852) and Proteintech (15168-1-AP) were used. The correct molecular weight of S1R is 25 kDa. GAPDH was used as loading control. The same membrane was reused for #74807 after stripping off sc-137075. (b) Illustration of magnetic-associated cell sorting (MACS) of glial cells from mouse cortex. ACSA-2, CD11b and NG2/O4/PDGFR α conjugated beads were used to purify astrocytes, microglia and OPCs, respectively. (c) Immunoblots with expression of S1Rs in sorted astrocytes, microglia and OPCs from mouse brain with CD11b and GFAP immunoblot demonstrating the purity of microglia and astrocyte from MACS respectively. α -Tubulin was used as loading control. Asterisk (*) indicates the band of α -Tubulin which was not totally stripped off. (d) Quantification of grey values of bands from c showing the relative expression of S1R proteins in different glial cells (normalized to α -Tubulin). $n = 3$ mice.



intensity (MFI) were performed using ZEN 3.0 SR (black edition) (Carl Zeiss, 16.0.2.306), no blinding was applied.

Four to five transversal sections per mouse were collected randomly from the cervical spinal cord. Three arbitrary areas from the white matter (WM) and grey matter (GM) were taken by confocal microscopy and analysed by ZEN 3.0 SR (black edition).

For the analysis of the SWI experiment, a custom-made ImageJ plugin LROI (<http://imagej.net/User:CIPMM-MolPhys>) was used. LROI creates a set of neighbouring, non-overlapping Regions of Interest (ROIs) with a specific width and height, along a user-drawn guidance line. The ROI height is determined by dividing the length of the guidance line by the number of ROIs to create.

After scanning with the epifluorescence microscope AxioScan. Z1, original images were exported and further processed in ImageJ (ImageJ 1.53q, NIH). The centre-point of guidance lines was aligned with the injury lesion core (as '0'). After creating 40 ROIs perpendicular to the lesion area (ipsi), another 40 ROIs were created on the corresponding contralateral (contra) side. For each side, the analysed 40 ROIs covered an area of $1200 \times 800 \times 30 \mu\text{m}$ (L \times W \times H). The LROI tool was used to quantify the mean fluorescence intensities (MFI) of S1R staining at once. Relative S1R expression levels were determined by MFI of ROIs of the ipsilateral side normalized to the counterparts of the contralateral side.

2.10 | Single-cell transcriptome analysis

A single-cell RNA sequencing (scRNA-seq) dataset in the Gene Expression Omnibus (GEO) database containing an expression matrix of whole brains from 2 to 3-month-old mice (GSE129788) was used for downstream analysis (Ximerakis et al., 2019). The Seurat package (v.4.1.1) was used for basic processing and visualization of the scRNA-seq data in R (v.4.2.0) (Stuart et al., 2019). Cells with genes less than 200 or more than 2500 or containing >10% of mitochondrial genes were excluded from analysis. The data were then normalized by the total expression before they were log-transformed. FindVariableFeatures function with default parameters was used to detect highly variable genes. Linear scaling was subsequently conducted. Unique molecular identifier (UMI) counts and a fraction of mitochondrial reads were removed using the ScaleData function. Cell type was determined as previously described (Ximerakis et al., 2019). Principal component analysis (PCA) was performed on the scaled data for dimensional reduction and top 20 principal components were included. Clusters were identified using the FindClusters function. Results were visualized with non-linear dimensional reduction method t-distributed stochastic neighbour embedding (t-SNE).

2.11 | Statistical analysis

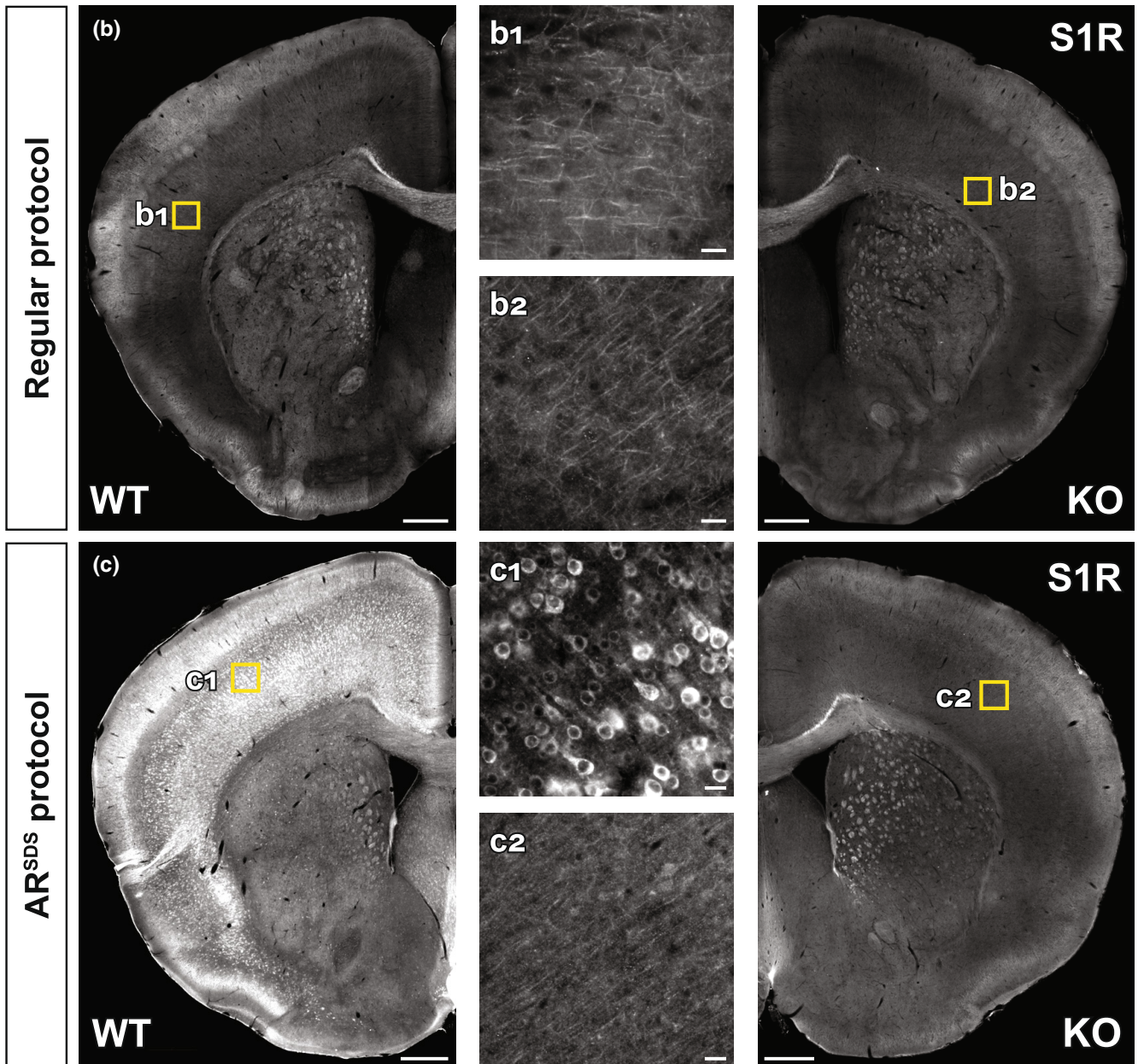
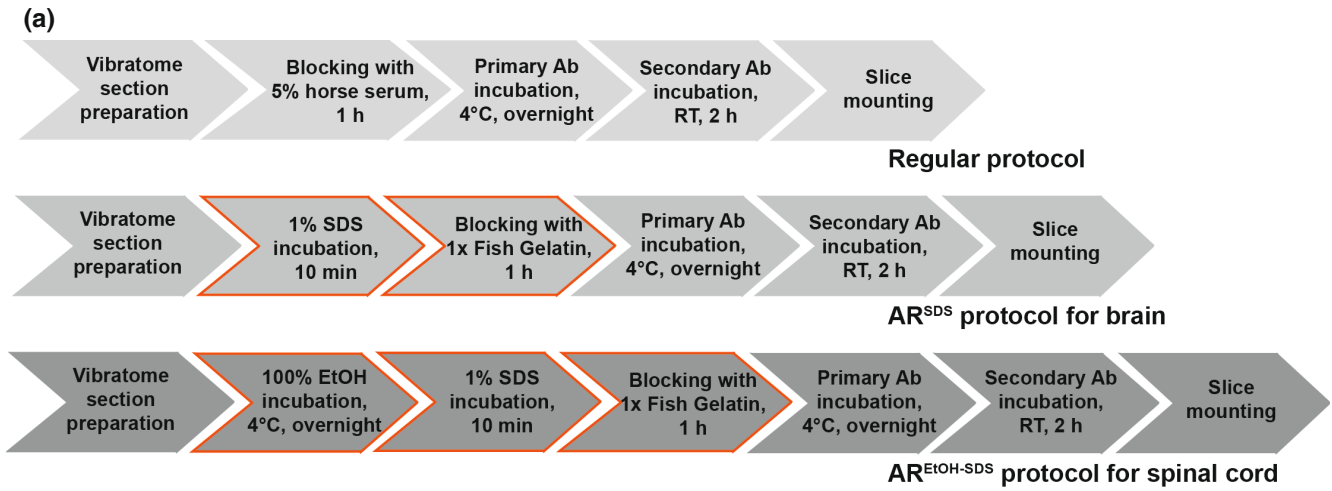
No statistical method was used to pre-determine sample size which was determined according to previous experience with the aim to minimize the animal numbers used for the experiments. No randomization was performed to allocate subjects in the study. No test for outliers was conducted, and no data point was excluded. Data were analysed using the GraphPad Prism 9.3.1 statistical software (GraphPad). All data points were used for analysis and were given as mean \pm SEM, n = mouse numbers. For statistical analysis the normality of data was assessed by the Shapiro-Wilk test, thereby two-tailed Student's *t*-test was used for comparison between two groups and one-way ANOVA for comparison among more than two groups followed by Tukey's post hoc test. *p* values of ≤ 0.05 were considered statistically significant. Based on our previous studies reaching statistically significant reduction of cell-type-specific gene ablations with an alpha value of 0.05 (Fang et al., 2022; Saab et al., 2016), we determined the sample sizes (three mice per group) in the current study showing the statistical significance of the loss of S1Rs in neuronal/microglial Cre-expressing mice. Therefore, no post hoc analysis was performed for the sample size power.

3 | RESULTS

3.1 | Specific detection of the S1R by immunoblot

To identify reliable S1R antibodies, we screened six commercially available antibodies on tissue homogenates obtained from the cerebral cortex and spinal cord of WT and S1R KO mice by immunoblotting. The protein samples were prepared by RIPA buffer containing 1% Triton X-100 to release total proteins of the tissue. We loaded 5–30 μg proteins per sample for SDS-PAGE. Prior to incubating with primary antibodies, we stained the blotted nitrocellulose (NC) membranes with Ponceau S solution to confirm proteins of different sizes were uniformly transferred. After incubating the NC membrane with S1R antibodies, we took advantage of the high sensitivity of the HRP (horseradish peroxidase)-based enhanced chemiluminescent (ECL) system to detect S1Rs. To detect potential unspecific signals, we exposed each membrane incubated with different S1R antibodies to a digital imaging system for as long as 15 min. We observed that one monoclonal rabbit antibody #61994 (Ab^{#61994}) from Cell Signaling showed strong signals at the expected size of the S1R (25 kD) in WT mice which were completely absent in the KO mice (Figure 1a, left). Even with the long exposure time (15 min), we

FIGURE 2 Establishing immunohistochemical protocols to specifically detect S1Rs. (a) Immunohistochemical protocols tested for vibratome sections of brain and spinal cord. The regular protocol without antigen retrieval (AR) was compared to AR^{SDS} protocol with AR using 1% SDS for brain slices. The modified AR^{SDS} protocol with AR using 100% ethanol and 1% SDS sequentially was used for spinal sections (AR^{EtOH-SDS}). (b, c) Fluorescent images of S1R immunostainings performed with the regular protocol (b) or AR^{SDS} protocol (c) using Ab^{#61994}. Magnified images (b1, b2, c1, c2) showing corresponded yellow boxes in the cortex of WT (b1, c1) and KO (b2, c2) mice. Scale bars = 200 μm in b-c, 5 μm in b1, b2, c1, c2.





detected only faint bands at positions of higher molecular weight. In addition, Ab^{#61994} generated the same immunoblot results to detect S1Rs in whole brain lysates (data not shown). Another monoclonal rabbit antibody #74807 from Cell Signaling did not show any bands at 25 kD but unspecific upper bands in WT and KO mice. The monoclonal mouse antibody sc-137075 from Santa Cruz showed relatively weak but specific bands of S1Rs at 25 kD, in line with previous studies (Moreno et al., 2014; Yang, Shen, Li, Stanford, & Guo, 2020). However, Ab^{sc-137075} also detected many other proteins of different sizes both in WT and KO mice. Other polyclonal rabbit antibodies, that is 42-3300 from Invitrogen, ab53852 from Abcam and 15168-1-AP from Proteintech, showed bands at 25 kD and other positions both in WT and KO mice (Ab^{15168-1-AP} showed weaker bands at 25 kD in KO mice), indicating unspecific detections of S1Rs by those antibodies for immunoblot (Figure 1a). Taken together, Ab^{#61994} was identified as the most specific antibody to detect S1Rs in CNS tissues by immunoblot.

Previous transcriptome profiling studies using purified cells from postnatal mice demonstrated that *Sigmar1* was widely expressed in neurons and glial cells, and was even detected with higher expression level in microglia and OPCs than in other cells (Figure S1A) (Zhang et al., 2014). To detect *Sigmar1* expression levels in glial cells of adult mice, we purified translated mRNA directly from astrocytes, microglia and OPCs of adult mouse cerebral cortex using a Cre-dependent RiboTag approach (Figure S1B,C,D). Quantitative real-time PCR (qPCR) results suggested that adult astrocytes, microglia and OPCs all expressed *Sigmar1* mRNA, however, with variable levels when normalized to the *Actb* expression per se (Figure S1E). To further confirm the S1R protein expression in adult glia, we purified astrocytes, microglia and OPCs from the cortex of adult WT mice by magnetic-activated cell sorting (MACS) and performed immunoblots with the specific Ab^{#61994} (Figure 1b-d). We observed that S1Rs could be detected in protein samples from purified astrocytes, microglia and OPCs. A comparison using α -tubulin as loading controls demonstrated that glial cells do express S1R proteins with variable levels. Notably, Western blot and qPCR analyses of target genes usually rely on normalization to expression levels of housekeeping genes (e.g. β -actin, α -tubulin) which are unequal in different cell types (Ximerakis et al., 2019; Zhang et al., 2014), thereby it is difficult to quantitatively compare S1R expression in purified CNS cells by these methods. Instead, *in situ* immunolabelling would help to better determine the expression pattern of the S1R.

3.2 | Establishment of a reliable protocol for S1R immunohistochemistry

To investigate the S1R expression *in situ*, a specific S1R antibody working for IHC is highly demanded. Because paraffin or cryo-section preparations are known to be harmful to antigen preservations for IHC (Hira et al., 2019; Shi, Cote, & Taylor, 1997), we used free-floating vibratome sections of formaldehyde-fixed brain tissues. We started with the regular protocol working well in our previous

studies (Huang et al., 2020; Huang, Guo, Bai, Scheller, & Kirchhoff, 2019) to test the S1R antibodies (Figure 2a). However, we observed that Ab^{#61994}, Ab^{#74807} (data not shown) and Ab^{sc-137075} did not show any labelling in WT and KO mice (Figure 2b and Figure S2A). We also found that Ab^{ab53852} and Ab^{15168-1-AP} showed weak immunostaining in neuron-like cell bodies which were identical in WT and KO mice (Figure S2B,C). In addition, Ab^{ab53852} and Ab^{15168-1-AP} strongly labelled many cells with a pattern very similar to anti-GFAP staining, mostly in corpus callosum and hippocampus of WT and KO mice. We noticed that such GFAP-like staining was the only immunolabel of Ab⁴²⁻³³⁰⁰, however, both in WT and KO mice (Figure S2D). Therefore, these S1R antibodies are not suitable for IHC and specific immunolabelling of cells in the mouse brain.

SDS has been suggested as an AR reagent for antibodies detecting denatured proteins in IHC (Brown et al., 1996; Wilson & Bianchi, 1999). Considering that Ab^{#61994} specifically recognized SDS-denatured S1Rs for immunoblot, we thereby treated vibratome brain slices with SDS (1%, 10 min at RT (20-22°C)) for AR prior to the blocking step (Figure 2a). And indeed, we observed bright and clear immunoreactivity to Ab^{#61994} in WT mice which was completely absent in S1R KO mice, strongly indicating the capability of Ab^{#61994} to specifically detect S1Rs in IHC (Figure 2c). Control experiments with only secondary antibodies further confirmed the reliable staining of Ab^{#61994} in WT mice (Figure S3A,B). Detailed analysis revealed the AR^{SDS} protocol (i.e., 1% SDS for AR+Ab^{#61994}) specifically detected S1R-expressing cells in all CNS regions, except some unspecifically stained white matter tracts in the brain stem, cerebellum and spinal cord (Figure S4A,B) which was not caused by Triton X-100 used in the blocking buffer that may generate myelin staining as suggested by previous studies (Figure S3C,D) (Weruaga et al., 1998). We also noticed that unlike previous reports (Mavlyutov et al., 2010), the cerebral cortex, hippocampus, thalamus and olfactory bulb area showed strong immunolabelling of S1Rs by this protocol (Figure S4A, a₁-a₃ and B, b₁-b₃). Although in images with higher magnifications a background staining of tiny puncta could be seen in WT and KO mice (Figure S5A), Ab^{#61994} immunolabelling clearly demonstrated the ER-like perinuclear ring structures of the S1R staining as reported in previous studies using EYFP-tagged S1Rs in cultured cells (Hayashi & Su, 2007; Kopanchuk et al., 2022) which was further confirmed by co-labelling an ER marker SERCA2 (Figure S5B). In addition, this protocol could immunolabel S1Rs in other organs such as liver (Figure S6A-D) and heart (Figure S6E-H). Therefore, the current AR^{SDS} protocol is able to reliably identify S1R expression *in situ*.

We tested the effect of 1% SDS pre-treatment for other S1R antibodies as well. However, we did not observe improved immunostaining by Ab^{#74807} (data not shown), Ab^{sc-137075}, Ab⁴²⁻³³⁰⁰ and Ab^{ab53852} compared to a treatment without SDS (Figure S7A-C). In line with the immunoblot results, the immunolabelling by Ab^{15168-1-AP} in WT mice was improved after the AR, whereas in KO mice similar but weaker immunostaining was also observed (Figure S7D). In addition, the GFAP-like staining pattern could always be found using Ab⁴²⁻³³⁰⁰, Ab^{ab53852} and Ab^{15168-1-AP} in WT and KO mice even after the AR (Figure S7B-D). Taken together, except Ab^{#61994}, the other

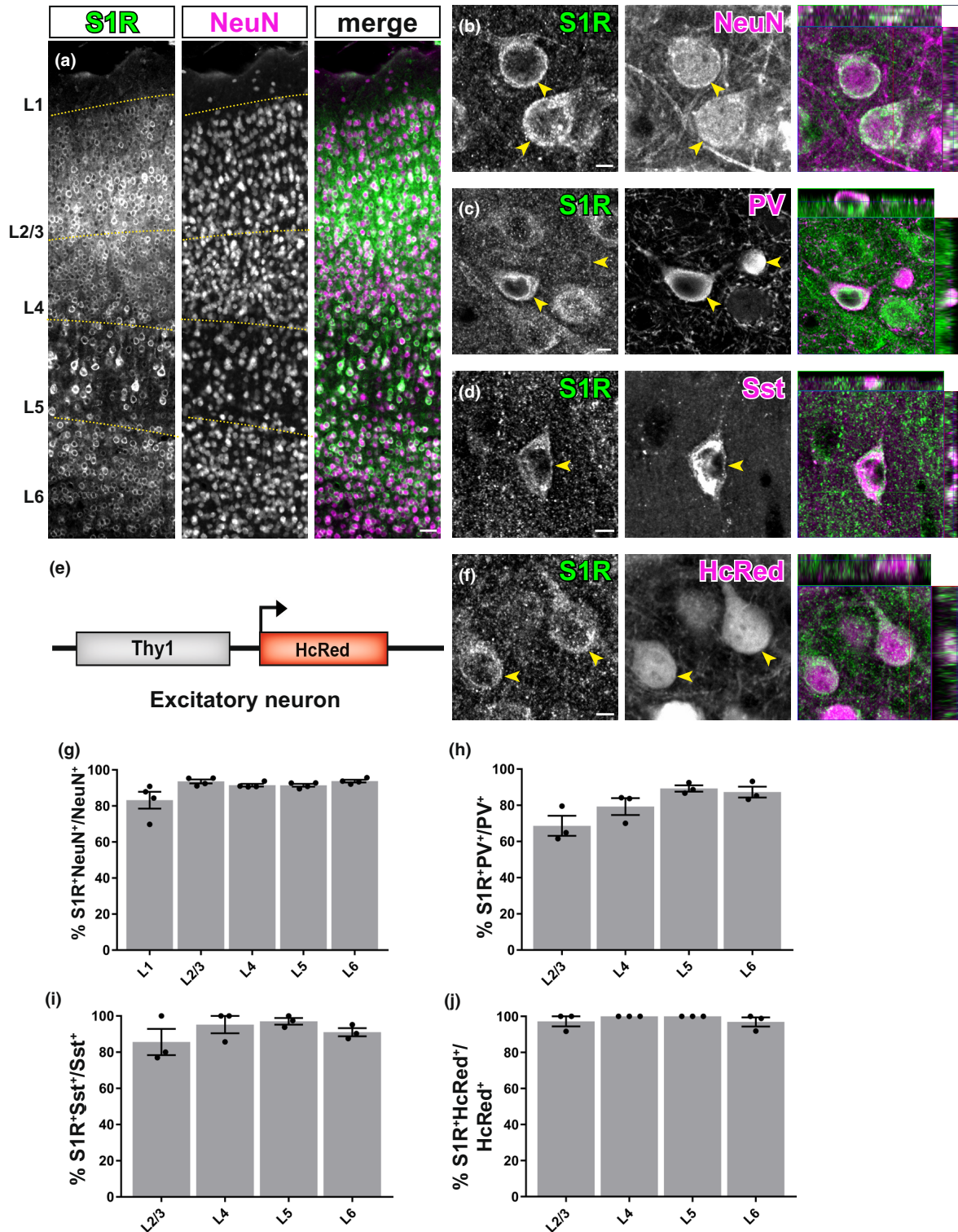


FIGURE 3 S1Rs are expressed abundantly in neurons. (a) Immunohistochemical detection of S1Rs in NeuN⁺ cells in different cortical layers (L1-L6). Almost all NeuN⁺ cells were co-localized with S1R immunolabelling. (b) Confocal images depicting the ring-like structure of S1R immunostaining in NeuN⁺ cells. (c, d) Detection of S1Rs in Parvalbumin⁺ (PV, c) and Somatostatin⁺ (Sst, d) interneurons. (e) Scheme with transgenic mice of Thy1-HcRed which were used to visualize excitatory neurons. (f) Confocal images showing the S1R immunoreactivity in HcRed⁺ excitatory neurons. The rightmost images of b,c,d,f show the orthogonal views. (g-j) The proportions of S1R⁺ cells in NeuN⁺ (g), PV⁺ (h), Sst⁺ (i) and HcRed⁺ (j) neurons from different cortical layers. *n* = 3 mice. Scale bars = 50 μm in (a), 5 μm in (b,c,d,f).

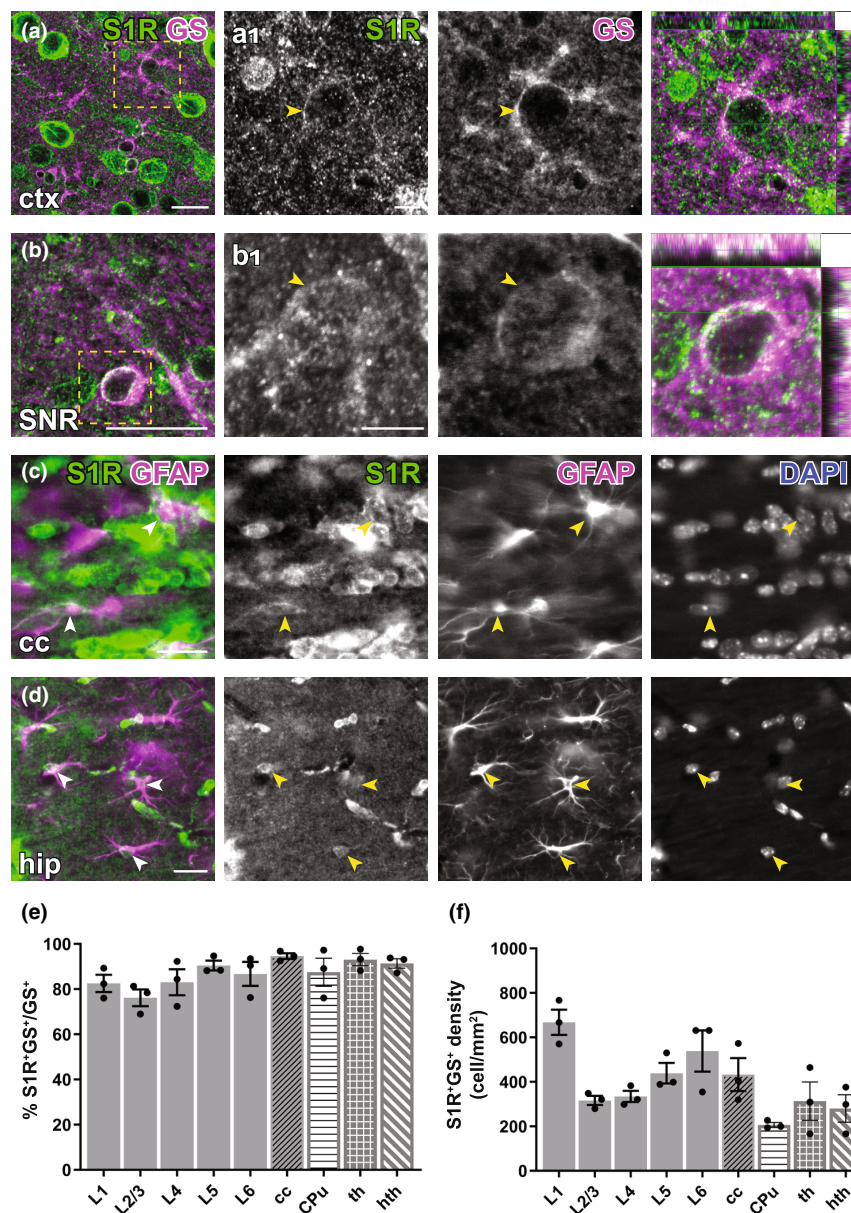


FIGURE 4 Immunohistochemical detection of S1R expression in forebrain astrocytes. (a, b) S1R immunoreactivities in GS⁺ astrocytes in ctx (a), substantia nigra (SNR, b). (a1–b1) Magnified images corresponding to boxed areas in (a, b). Arrowhead indicated S1R staining in astrocytes. The orthogonal views are shown in the rightmost pictures. (c, d) Axioscan images showing the ring-like structure of S1R staining in GFAP⁺ astrocytes in the corpus callosum (cc, c), hippocampus (hip, d). (e, f) Quantification of proportions and densities of GS⁺ cells expressing S1R⁺ in different cortical layers (L1–L6), cc, striatum (CPu, caudate putamen), thalamus (th) and hypothalamus (hth). *n* = 3 mice. Scale bars = 20 μ m in (a–d), 5 μ m in (a1–b1).

commercial S1R antibodies failed to provide a reliable immunolabelling of S1Rs for IHC.

3.3 | S1Rs are widely expressed in neurons and glial cells in the forebrain

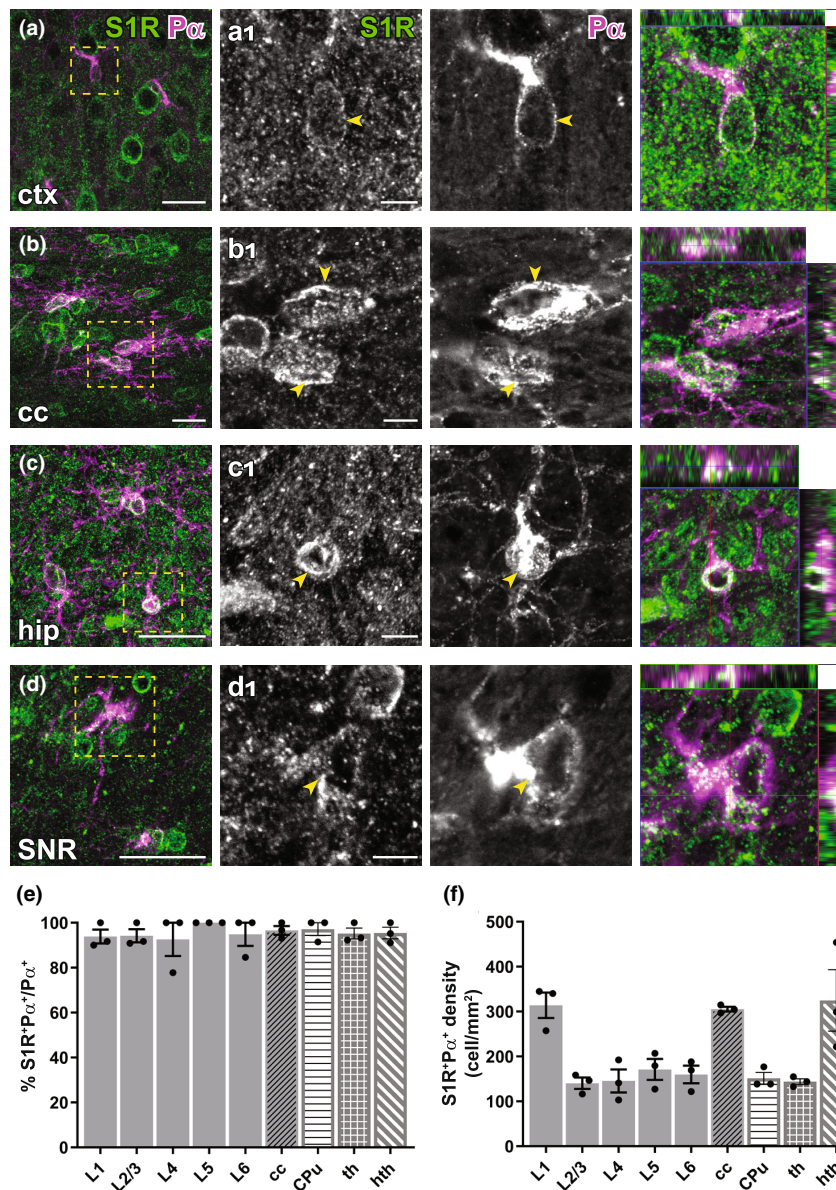
We took advantage of the newly established IHC AR^{SDS} protocol to study the expression of S1Rs in the CNS. We observed similar patterns of S1R immunoreactivity in the brains of mice at different ages from postnatal day 7 (P7) to 24 w (Figure S8A–D). Recent single-cell RNA sequencing (sc-RNA-seq) studies suggest that *Sigmar1* expression can be detected in CNS cell types with different proportions and levels (Figure S9) (Consortium, 2020; Ximerakis et al., 2019). Thus, we performed co-immunostaining for S1Rs and different cell markers in the brain of 8-week-old mice to study S1R expression in detail, with

particular focus on regions in the dorsal brain such as cerebral cortex (grey matter) and corpus callosum (cc, white matter) as well as in the ventral brain such as striatum (CPu, caudate putamen), thalamus (th) and hypothalamus (hth) (Figures 3–7).

We combined NeuN (a pan-neuronal marker) and S1R immunostaining to evaluate the expression of S1Rs in neurons. We found that throughout the forebrain, the majority of neurons were immunopositive for S1R (Figure 3a,b). For example, in all cortical layers, S1R immunolabelling was found in ~85% of NeuN⁺ cells in layer 1 (L1) and in more than 90% of NeuN⁺ cells in L2–6 (Figure 3g). Since NeuN also labelled interneurons in addition to principal excitatory neurons, we further studied the expression of S1Rs in two major interneuron types, i.e. parvalbumin (PV)⁺ and somatostatin (Sst)⁺ interneurons (Figure 3c,d). We found still the majority of PV⁺ or Sst⁺ interneurons were expressing S1R, however, with different proportions. Specifically, the proportion of PV⁺ interneurons



FIGURE 5 Detection of the S1R expression in OPCs in the forebrain. (a–d) S1R immunostaining co-localized with PDGFR α (P α) OPCs in ctx (a), cc (b), hip (c), SNR (d). (a1–d1) Magnified images showing boxed areas from (a–d). Arrowhead indicated S1R staining in OPCs. The rightmost images indicating the orthogonal views. (e, f) Quantification of proportions (e) and densities (f) of S1R⁺P α ⁺ cells in different cortical layers (L1–L6), cc, CPu, th and hth. $n = 3$ mice. Scale bars = 20 μ m in (a–d), 5 μ m in (a1–d1).



immunolabelled for S1R was ~70% in L1, ~80% in L2/3 and ~90% in L5 and L6 (Figure 3h), while ~90% of Sst⁺ interneurons showed immunoreactivity of S1R in L2–L6 (Figure 3i). Please note, virtually no PV⁺ or Sst⁺ cells were found in L1. To determine the S1R expression in excitatory neurons, we performed S1R immunostaining on brain slices from fluorescent transgenic mice in which excitatory neurons were labelled by HcRed expression driven by the Thy1 promoter (Figure 3e,f). In line with the results from NeuN⁺ cells, virtually all HcRed⁺ cells were found to be S1R immunopositive across the whole cortex (Figure 3j).

For detection of astrocytes, we used glutamine synthetase (GS) immunostaining. We observed that although the perinuclear ring structure of S1R in GS⁺ cells appeared thinner than in neurons, still most of GS⁺ cells in different areas across the forebrain could be immunolabelled for S1R (Figure 4a,b). We found ~80–90% GS⁺ cells expressing S1R in cortical layers, cc, CPu, thalamus and hypothalamus (Figure 4e,f). Notably, we did not find an S1R staining in

astrocytes that mimicked a typical GFAP-containing cytoskeleton well known from anti-GFAP immunostainings in the healthy brain (Figure 4c,d).

To study S1R expression in oligodendrocyte lineage cells, we performed PDGFR α (P α , an OPC marker) and APC CC1 (an OL marker) immunostainings. With the AR^{SDS} protocol, we were able to detect S1R expression in almost all OPCs (Figure 5) and OLs (Figure 6), both in grey matter (e.g. the cortex) and in white matter (e.g. the cc) as well as in other studied ventral brain areas. To our knowledge, this is the first time that S1R expression has been observed in OPCs by immunolabelling.

To study the microglial expression of S1Rs, we combined Iba1 (a microglia marker) and S1R immunostaining. Like other glial cells, the majority of Iba1⁺ cells were immunolabelled for S1R in all regions of the forebrain (Figure 7a–d). Quantification results even suggested that virtually all Iba1⁺ cells were co-expressing S1Rs, at least in the cortex, cc, CPu, thalamus and hypothalamus (Figure 7e–f).

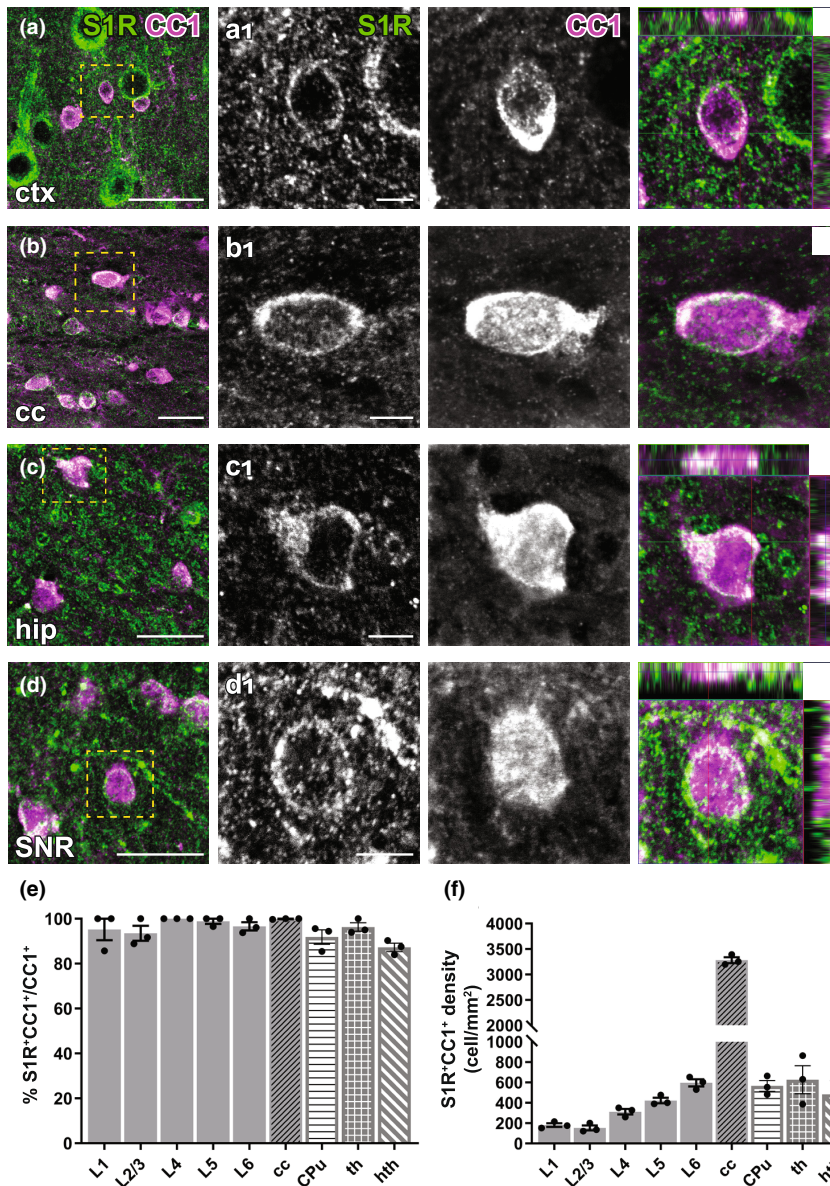


FIGURE 6 Immunohistochemical detection of S1Rs in forebrain oligodendrocytes. (a–d) S1Rs immunoreactivity in CC1⁺ oligodendrocyte in ctx (a), cc (b), hip (c), SNR (d). (a1–d1) Magnified images correspond to boxed areas in (a–d). Arrowhead indicated S1R immunostaining in oligodendrocyte. The orthogonal views are shown in the rightmost images (e, f) Quantification of proportions (e) and densities (f) of S1R⁺CC1⁺ cells in different cortical layers (L1–L6), cc, CPU, th and hth. $n = 3$ mice. Scale bars = 20 μm in (a–d), 5 μm in (a1–d1).

The specific S1R immunolabelling allowed us to compare relative expression levels of the S1R in different CNS cell types in defined regions *in situ*, for example, a comparison of individual cellular S1R expressions in deep cortical layers (Figure S10). Taken together, we were able to demonstrate that unlike previous scRNA sequencing results (Figure S9) the majority of neurons and all types of glial cells express S1R proteins with variable levels.

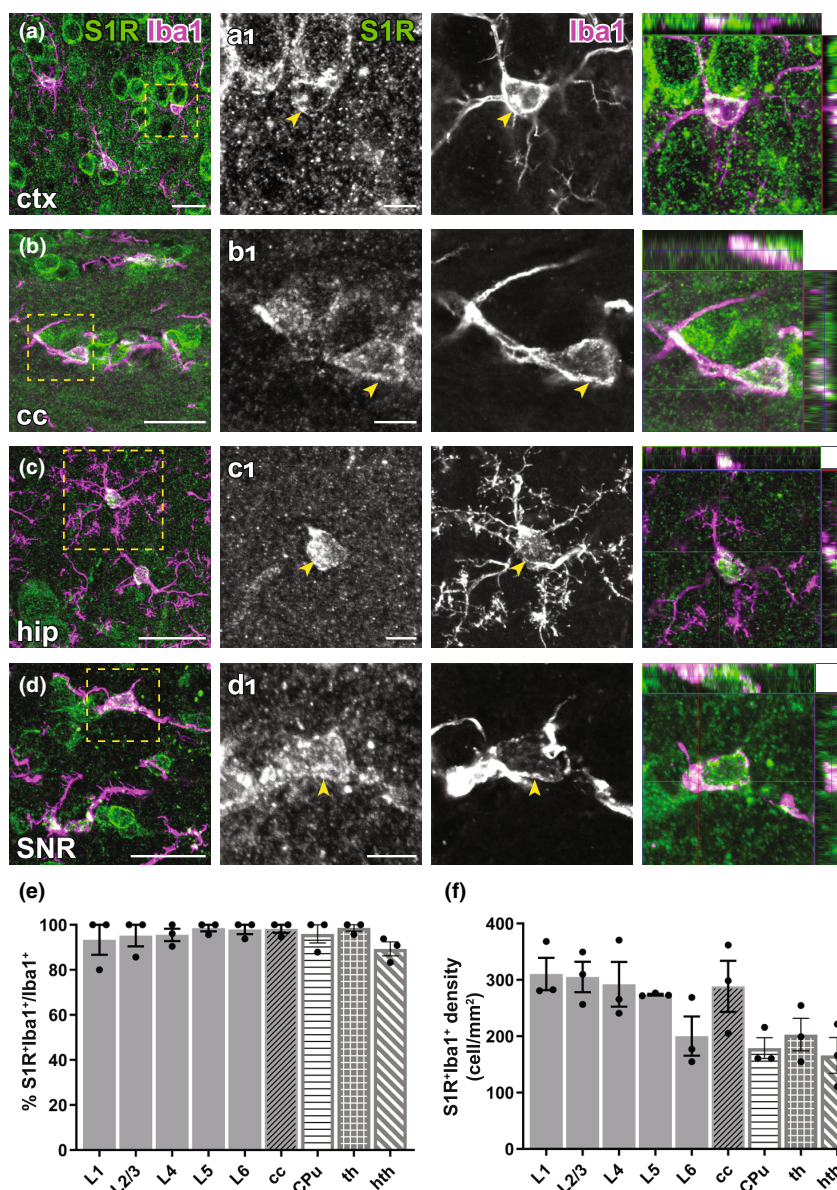
3.4 | S1Rs are widely expressed in the cerebellum and spinal cord

The AR^{SDS} protocol for S1Rs also generated specific immunolabelling of S1Rs in the cerebellum (Figure 8a,b). We observed high expression in cell bodies and neurites of Purkinje neurons (confirmed by Calbindin staining) (Figure 8c). Further investigations with other cell type markers revealed that S1Rs were widely expressed in

astrocytes including Bergmann glia (S100B⁺), microglia (Iba1⁺), OPCs (Pax⁺) and OLs (CC1⁺) in the cerebellum (Figure 8d–g).

Previous studies using Ab^{Ruoho} showed that high expression of S1R in motor neurons of the spinal ventral horn, however, the S1R expression in other cell types had not been mentioned. In the current work, we first tested the performance of the AR^{SDS} protocol for S1Rs in the spinal cord (Figure S11A). We observed high expression of S1Rs in the ventral horn of WT mice, but with a strong background. Moreover, unspecific staining by the AR^{SDS} protocol could also be observed in the KO mice, preferentially in white matter myelin structures. Considering delipidation of myelin is widely used to decrease background for the detection of myelin proteins (Ishii, Fyffe-Maricich, Furusho, Miller, & Bansal, 2012; Jahn, Tenzer, & Werner, 2009), we tested a pre-treatment of spinal slices with 100% ethanol overnight (more than 16 h), followed by 1% SDS treatment. This modified protocol (AR^{EtOH-SDS}, i.e., 100% ethanol +1% SDS+Ab^{#61994}; Figure 2a), largely reduced the background

FIGURE 7 Immunolabelling of S1Rs in microglia in the forebrain. (a–d) S1R immunolabelling colocalized with Iba1 staining in ctx (a), cc (b), hip (c), SNR (d). (a1–d1) Magnified images corresponding to boxed regions in (a–d). Arrowhead indicated overlapping of S1R and Iba1 immunostaining in microglia. The orthogonal images are presented at the rightmost. (e–f) Proportions (e) and densities (f) of S1R⁺Iba1⁺ cells in different cortical layers (L1–L6), cc, CPu, th and hth. $n = 3$ mice. Scale bars = 20 μm in (a–d), 5 μm in (a1–d1).



staining both in WT and KO mice (Figure S11B). Therefore, we performed co-immunostaining for S1Rs and glial markers with the AR^{EtOH-SDS} protocol on spinal sections. We found that virtually all neurons in the spinal cord, though with even higher level in the ventral horn, were expressing S1Rs (Figure S11C,D). Regarding the still relatively higher immunostaining background in the spinal cord compared to the brain, we quantified S1R immunopositive cells in WT and KO spinal cords. We found that more than 90% of all types of glial cells either in the spinal grey matter or white matter of WT mice were immunolabelled for S1R, whereas this proportion was no more than 5% in the KO mice (Figure S12 and S13). Therefore, this AR^{EtOH-SDS} protocol still could be used to specifically detect S1R-expressing cells in the spinal cord. However, for yet unknown reasons, the myelin-like staining could still be seen in both groups of mice with the AR^{EtOH-SDS} protocol. To further investigate the unspecifically stained components, we combined myelin basic protein (MBP, a myelin marker) and S1R

immunostaining. The unspecific S1R immunolabelling did not fully overlap with MBP staining, but appeared to be in the inner layers of myelin sheaths (Figure S11E,F). Thereby, this protocol is not suitable to study S1R expression in myelin in the spinal cord. More efforts are required to improve the AR of spinal slices for S1R immunostaining. Nevertheless, the current results from the AR^{EtOH-SDS} protocol demonstrated that the majority of neurons and glial cells in the spinal cord express S1Rs.

3.5 | Detection of S1Rs in the injured brain by immunohistochemistry

It has been suggested that S1R plays important role in the injured brain. However, the S1R expression pattern under neuropathology was not yet clear because of the lack of a reliable immunodetection method. Therefore, we evaluated the performance

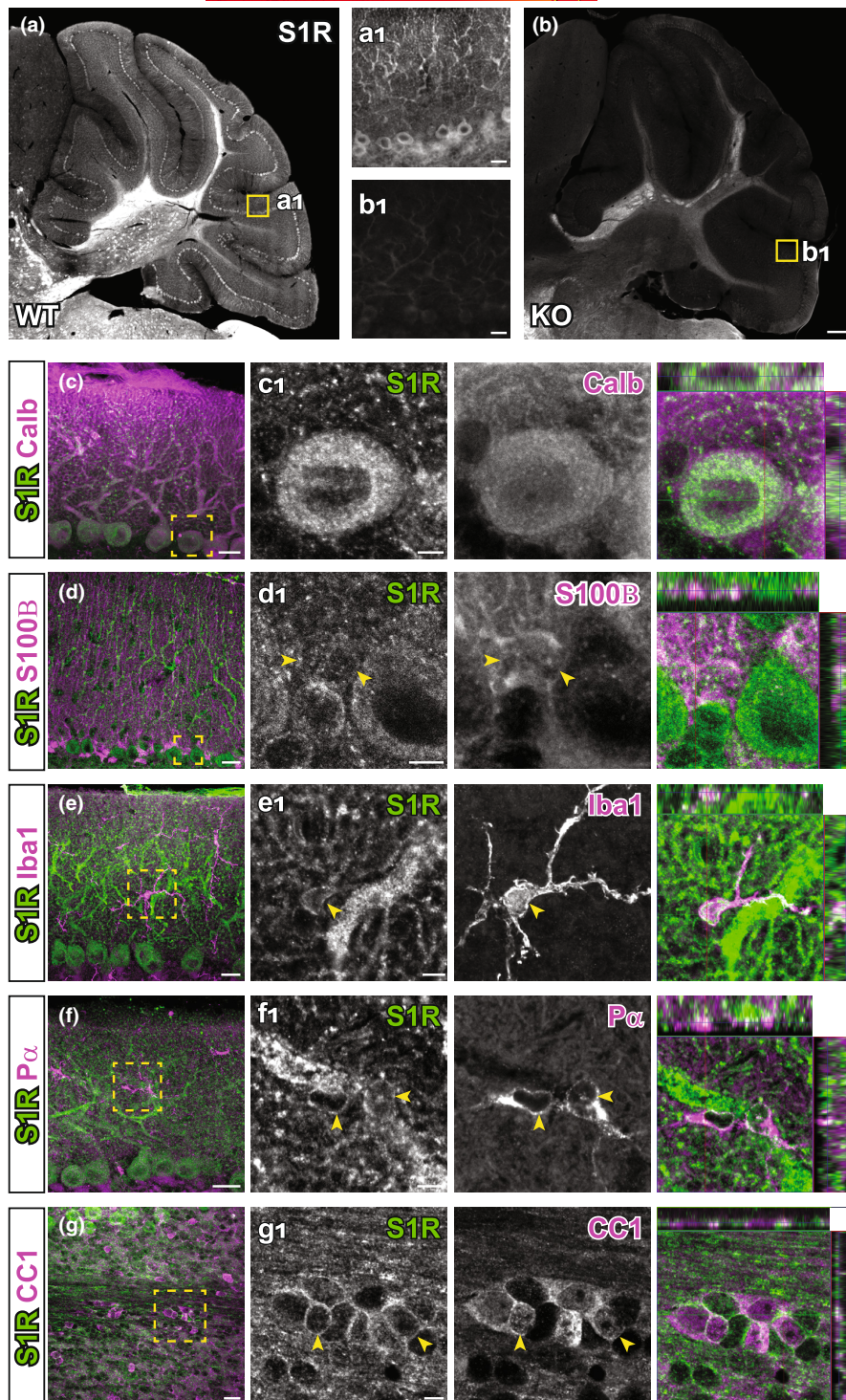
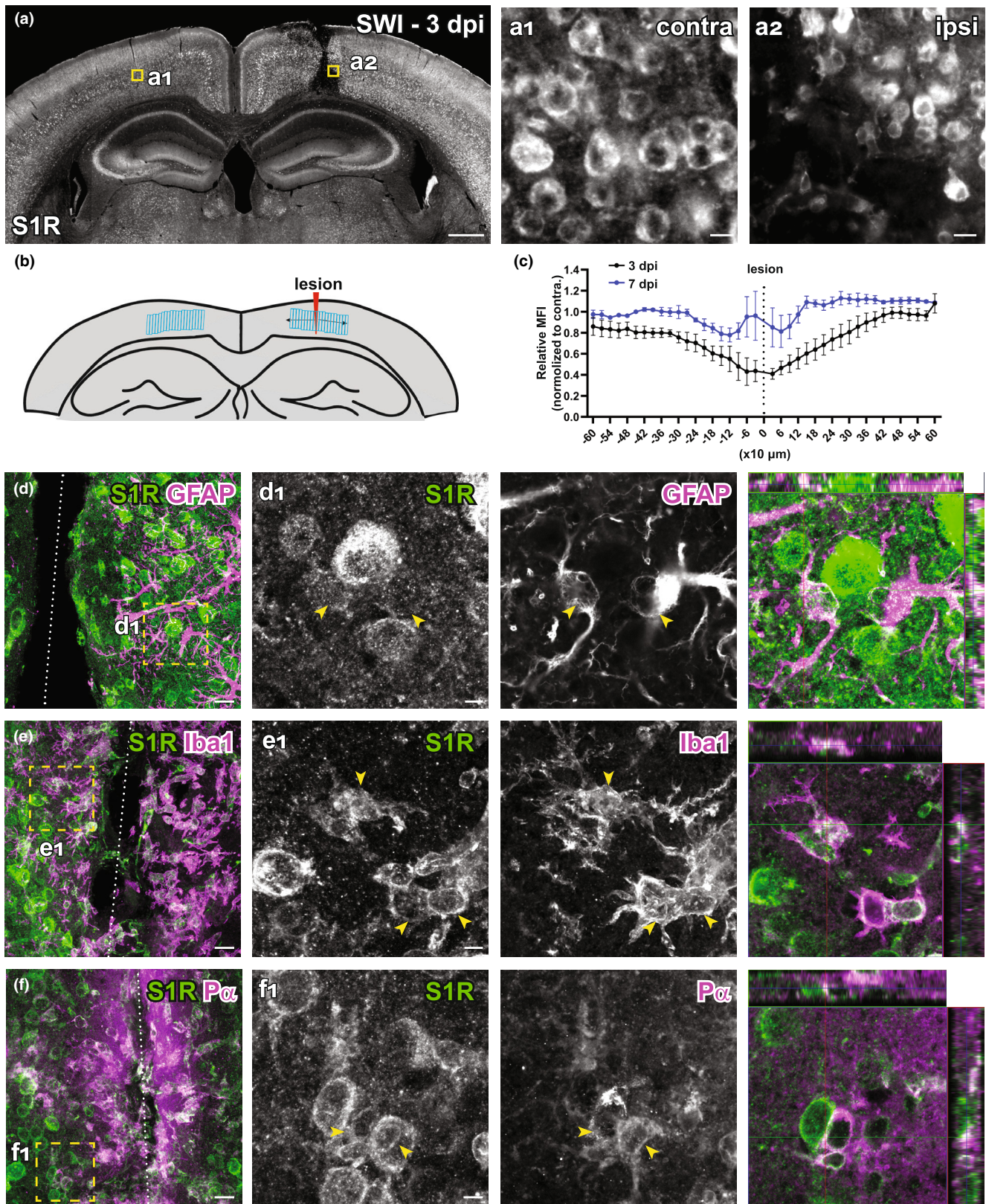


FIGURE 8 The expression of S1Rs in the cerebellum. (a, b) Sagittal sections of cerebellum were stained for S1R using the AR^{SDS} protocol. Specific immunostaining of S1Rs in WT cerebellum (a) is absent in S1R KO mouse (b). (a1, b1) Magnified views showing the molecular layer in the indicated regions of a and b. (c-g) Cerebellar slices were double-immunostained for S1Rs, calbindin⁺ (calb) (c), S100B⁺ (d), Iba1⁺ (e), P α ⁺ (f) and CC1⁺ (g) respectively. (c1-g1) The enlarged images of boxed area in (c-g). Scale bars = 200 μ m in (a, b), 20 μ m in a1, b1, c-g and 5 μ m in (c1-g1).

of the newly established S1R immunolabelling AR^{SDS} protocol working on brains with acute brain injuries. We performed cortical stab wound injuries (SWI) to adult mice which were analysed

at 3 and 7 days post-injury (dpi). The IHC results showed that S1Rs in the (peri-) injured area were still well detected by the current protocol. We observed that the S1R expression level in

FIGURE 9 Immunolabelling of S1Rs in the injured brain. (a) Overview of S1R immunostaining at 3 days post stab wound injury (3dpi). Ring-like structures of S1Rs in the contralateral (contra, a1) and ipsilateral (ipsi, a2) sides as indicated by the yellow boxes in a. (b) Schematic diagram showing the analysed area defined by LRoi. Regions of Interest (ROIs) were created perpendicular to the lesion. The lesion was chosen as the ROI 0 to be in the centre of all ROIs. Corresponding ROIs were created on the contralateral side. Distances of ROIs to the lesion site (defined as 0) were shown in x-axis. (c) Relative mean fluorescence intensity (MFI) of S1R immunostaining in ROIs from the injured side (ipsi) normalized to contralateral side at 3 and 7 dpi respectively. (d-f) Injured brain sections were co-immunostained for S1Rs with various glial markers (GFAP, Iba1 and P α). (d1-f1) The boxed areas in d-f are magnified. Activated astrocytes (GFAP⁺), microglia (Iba1⁺) and OPCs (P α ⁺) at the lesion site were expressing S1Rs enriched in the cell body. Scale bars = 500 μ m in a, 10 μ m in a1-a2, 20 μ m in d-f and 5 μ m in d1-f1.



the ipsilateral cortex did not show overt difference compared to the contralateral side, although the core injury area showed reduced S1R expression possibly because of loss of neurons (contra, Figure 9a,a1; ipsi, Figure 9a,a2) at 3 dpi which partially recovered with the wound healing at 7 dpi (Figure 9b,c). Moreover, S1Rs

were also detected in activated microglia, astrocytes and OPCs in the injury-affected region (Figure 9d-f). Of note, we still did not find S1R immunostaining colocalized with GFAP in the main processes of astrocytes (Figure 9d,d1). Compared to resting microglia in healthy brain, activated microglia showed stronger S1R

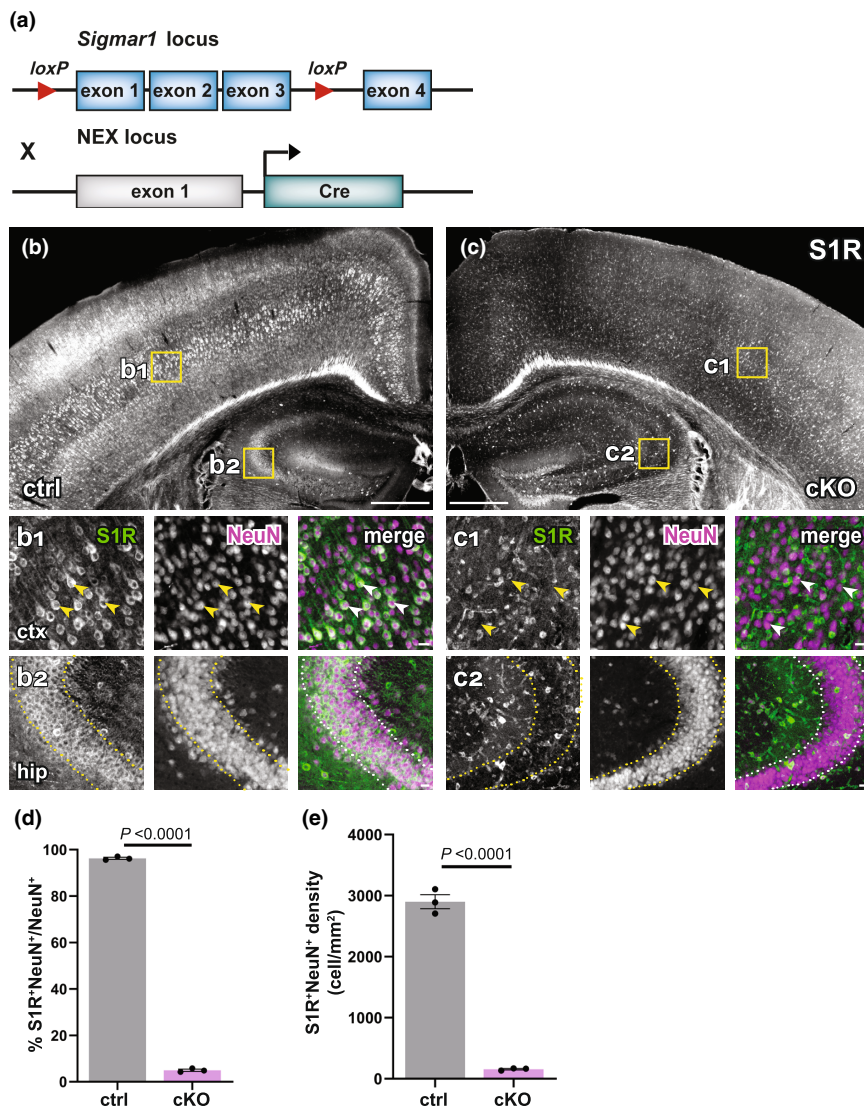


FIGURE 10 Successful knockout of S1Rs in principal neurons within the neocortex and hippocampus. (a) Scheme with transgenic structures of NEX-Cre x S1R^{fl/fl} mice used to delete S1Rs in principal neurons. (b, c) Overviews of S1R immunostaining in the dorsal brain of control (ctrl, b) and cKO (c) mice. (b1, b2, c1, c2) Magnified views (yellow boxes in b and c). Arrowheads indicate reduced S1R expression in cortical NeuN⁺ cells in cKO (c1) compared with ctrl (b1). Dotted lines indicate reduced expression of S1Rs in pyramidal neurons in the hippocampal CA2 region of cKO (c2) compared with ctrl (b2) mice. (d–e) Histograms highlighting decreased proportion and density of S1R⁺ cells in NeuN⁺ cells in cKO mice. $n = 3$ mice per group. Scale bars = 500 μm in (b, c), 50 μm in b1–b2, c1–c2.

expression, though its biological meaning remains to be elucidated (Figure 9e,e1).

3.6 | Conditional deletion of S1Rs in the CNS in vivo

The newly established IHC protocol detecting S1Rs specifically enabled us to show that S1Rs are widely expressed in neurons and glial cells in the CNS. Therefore, the conditional knockout of S1Rs in cell types of interest in vivo would be a valuable tool to study S1R functions in the CNS. To achieve this goal, we generated a S1R flox mouse in which the exons 1–3 of *Sigmar1* are flanked by loxP sites (Figure S14). To test whether S1Rs could be specifically deleted in neurons in vivo, we crossed S1R flox mice to NEX-Cre knockin mice in which principal neurons express Cre to generate neuronal S1R cKO mice (NEX-Cre x S1R^{fl/fl}) (Figure 10a). Control mice (NEX^{wt/wt} x S1R^{fl/fl}) and cKO mice were analysed at 10 w. We were able to show that S1R expression was drastically reduced in

pyramidal neurons in the expected brain regions such as neocortex and hippocampus (Figure 10b,c). Quantification of S1R-expressing NeuN⁺ cells in the dorsal cortex confirmed that either in proportion (~96% in ctrl, ~5% in cKO) or in density (2900 cells/mm² in ctrl, 156 cells/mm² in cKO) S1R expression was largely ablated in NeuN⁺ cells in the neuronal S1R cKO mice ($t = 142.7$, $df = 4$, p -value < 0.0001 in d and $t = 23.65$, $df = 4$, p -value < 0.0001 in e) (Figure 10d,e).

To evaluate the temporally controlled deletion of S1Rs in targeted cell types of S1R flox mice, we crossbred S1R flox mice to CX3CR1-CreERT2 mice (CXCT^{t2/wt} x S1R^{fl/fl}) to generate microglia-specific S1R cKO mice (Figure 11a). These mice were injected with tamoxifen at 4 w and analysed at 3 or 6 w post-injection (wpi) (Figure 11b). Upon quantification of the immunostaining for Iba1 and S1R, we observed that in the dorsal cortex of cKO mice the proportion of Iba1⁺ microglia co-expressing S1R was reduced to $34.8 \pm 2.9\%$ at 3 wpi compared to ctrl ($96.4 \pm 3.2\%$). This level did not further decrease at 6 wpi ($29 \pm 6\%$) ($F[2, 6] = 76.61$, p -value < 0.0001) (Figure 11c–f). Thereby, we conclude that in adult

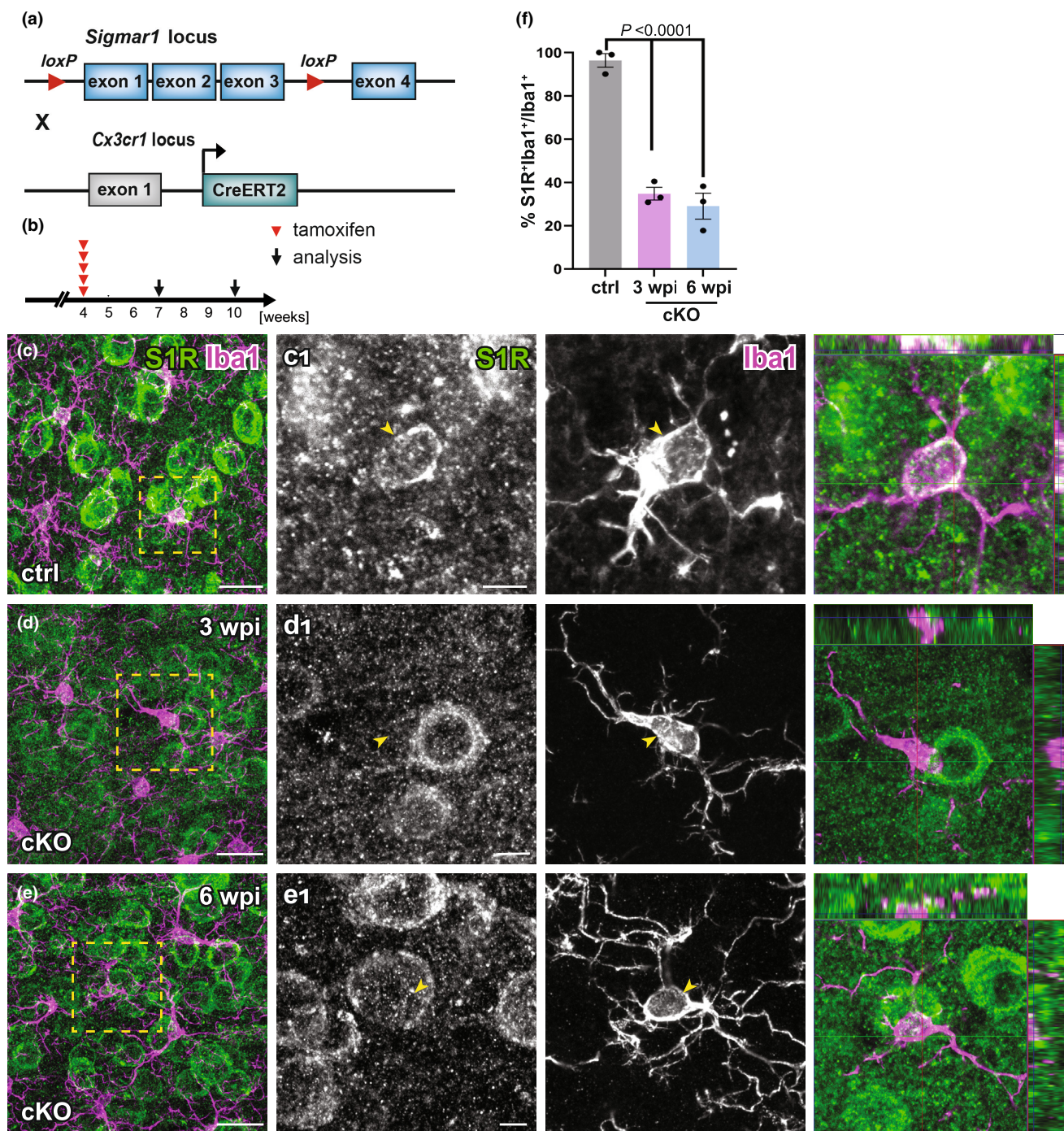


FIGURE 11 Successful deletion of S1Rs in microglia. (a) Schematic representation of double transgenic mice *CX3CR1-CreERT2* × *S1R^{fl/fl}* used to conditionally delete S1Rs in microglia. (b) Experimental plan. All mice were injected with tamoxifen at 4 w. Immunostaining of S1Rs was performed at 3 w (3 wpi) or 6 w (6 wpi) post the first tamoxifen injection. (c–e) Double-staining of S1R and Iba1 in ctrl (c) and cKO (d–e) mice. (c1–e1) The boxed regions from c–e are magnified. The orthogonal views of S1R and Iba1 immunolabelling are presented in the images at the right (f) Quantification S1R-expressing Iba1⁺ microglia in the ctx of ctrl and cKO mice. $n = 3$ mice per group. Scale bars = 20 μ m in c–e, 5 μ m in c1–e1.

mice the microglial S1R expression can be largely deleted within 3 weeks upon Cre induction.

Taken together, the S1R flox mouse appears as a powerful tool to efficiently delete S1Rs in neurons and glial cells in the CNS in vivo.

4 | DISCUSSION

Validation in KO animals is a golden standard to verify the specificity of antibodies for immunoblot and immunolabelling (Laflamme et al., 2019). After screening of six commercial S1R antibodies using



S1R KO mice, we identified Ab^{#61994} from Cell Signaling as a reliable antibody for specific detection of S1R using Western blotting of brain and spinal cord lysates. Ab^{#61994} is a newly produced rabbit monoclonal antibody, which has been used only in a few studies so far (six publications according to the Cell Signaling website). Recently, one study by Abdullah et al., verified the specificity of Ab^{#61994} to detect S1Rs in tissue lysate from mouse heart, but without showing the complete protein separation range of the immunoblot (Abdullah et al., 2020). Therefore, the current work provides further evidence that Ab^{#61994} is a reliable antibody specifically recognizing S1Rs in immunoblot without generating bands at other molecular weight positions. However, four other S1R antibodies showed bands in protein samples from both WT and KO mice, indicating they are not working specifically for immunoblot. The antibody sc-137075 from Santa Cruz showed specific bands of S1Rs at the correct size, but also unspecifically bound to many proteins with different sizes other than S1Rs. Furthermore, we identified that only Ab^{#61994} could generate specific immunohistochemical staining of S1Rs with AR by 1% SDS. The other S1R antibodies failed to generate specific immunostaining *in vivo* under our tested conditions. Thus, our results suggest to cautiously re-evaluate previous studies using those antibodies for immunoblot, immunoprecipitation and/or IHC of S1Rs.

The S1R has been discovered for over 40 years. Intensive *in vitro* studies have revealed that S1Rs are serving as a pluripotent modulator of various cellular functions and are ligand-operated chaperons mainly localized on the ER membrane (Su et al., 2016). Recent transcriptomic studies of either bulk sequencing of purified CNS cells or single-cell sequencing all suggest that the S1R mRNA is widely detected in different cell types in the CNS (Consortium, 2020; Ximerakis et al., 2019; Zhang et al., 2014). However, the spatial protein expression pattern of S1R is still difficult to conclude because of conflicting IHC results using antibodies generated by different research groups or commercial companies (Alonso et al., 2000; Hayashi & Su, 2004; Palacios et al., 2003). A recent study using S1R KO mice examined the specificity of the Ab^{Ruoho} and several commercial S1R antibodies including Ab^{sc-137075} and Ab⁴²⁻³³⁰⁰ for IHC in dorsal root ganglion (DRG), which suggested only Ab^{Ruoho} could reliably label S1Rs in the DRG (Mavlyutov et al., 2016). Furthermore, Ab^{Ruoho} was the only antibody validated by S1R KO mice for immunolabelling of S1Rs in the CNS, though it did not work well for immunoblot (Mavlyutov et al., 2010; Mavlyutov et al., 2016). However, IHC studies using Ab^{Ruoho} did not provide a clear S1R expression pattern at (sub)cellular levels in the CNS *in vivo*. In addition, Ab^{Ruoho} is a custom-made antibody, hence, with limited availability to the research community.

In the current study, the newly established IHC protocol (AR^{SDS} protocol) using Ab^{#61994} clearly revealed that S1Rs are mainly localized in the ER-like structure of CNS cells as suggested by *in vitro* studies. Notably, unlike the study using the Ab^{Ruoho} (Mavlyutov et al., 2016) the current protocol demonstrated high expression levels of the S1R in the olfactory bulb, cerebral cortex, hippocampus and thalamus. Combining immunostainings with cell type-specific markers, we were able to show that in addition to neurons, as suggested

by using Ab^{Ruoho} (Mavlyutov et al., 2010), S1Rs are widely expressed in various glial cells in the CNS including astrocytes, OPCs, OLs and microglia. Several AR methods such as heating with citrate buffer, microwave treatment, etc., have been tested to improve the immunostaining quality for the S1R in cultured cells (Hayashi, Lewis, Hayashi, Betenbaugh, & Su, 2011). In the current study, 1% SDS was used for the AR of the formaldehyde-fixed CNS tissue, substantially improving the S1R immunostaining. However, no AR was performed in studies using Ab^{Ruoho} (Mavlyutov et al., 2016; Nakamura et al., 2019), which may explain their relatively fainter staining of S1Rs in the CNS compared to the results of the current protocols. Even more importantly, Ab^{#61994} is a monoclonal antibody produced by immortalized hybridoma cells, thereby ensuring its sustainable availability to the research community.

Although Ab^{#61994} displayed a very good capacity to specifically detect S1Rs in immunoblot and IHC, some drawbacks of using this antibody have to be considered. First, regarding the punctate background signals in the S1R KO brain, the signal/noise ratio of the current IHC protocol was not satisfactory to identify potential S1R expressions in fine structures such as the plasma membrane upon stimulations by agonists or stress *in vivo* (Su et al., 2016). Second, Ab^{#61994} can unspecifically bind to myelin-like structures in the spinal cord, brain stem and cerebellar white matter, hence limiting its application in white matter studies in certain CNS regions. Third, Ab^{#61994} did not work for IHC in brain tissues without SDS treatment, indicating that Ab^{#61994} may only recognize denatured S1R proteins. Therefore, it would be difficult to immunoprecipitate naïve S1Rs using Ab^{#61994}. Further optimization of AR protocols for Ab^{#61994} as well as newly designed S1R antibodies would help to solve such problems.

Activation or inactivation of S1Rs by exogenous ligands both showed therapeutic effects for numerous neurological and psychological disorders. However, endogenous ligands of the S1R still remain unclear, hindering the understanding of patho- as well as physiological roles of the receptor *in vivo* (Sałaciak & Pytka, 2022; Schmidt & Kruse, 2019). Loss-of-function experiments would be an ideal strategy to investigate functions of S1R. However, unlike the pharmacological effects of the exogenous ligands, S1R KO mice showed mild phenotypes in ageing-related memory loss, cognitive impairments, motor defects, etc. (Couly et al., 2022). One possible explanation to such discrepancy can be a certain genetic compensatory machinery established during embryonic development that rescues the loss of S1R functions in global KO mice (El-Brolsy & Stainier, 2017). For example, hepatocyte-specific SIRT1 cKO mice develop a fatty liver which was not seen in global SIRT1 KO mice (Wang, Li, & Deng, 2010). Moreover, neither pharmacological intervention nor constitutive deletion of S1R could exclusively study S1R functions in specified cell types. To address such questions, we generated a Cre-dependent S1R conditional KO mouse (S1R flox). For the proof of concept, we showed that S1Rs could be successfully deleted in neurons or microglia mediated by Cre or CreER/tamoxifen systems *in vivo*. Regarding the broad expression of S1R in various cell types in and outside of the CNS, this newly generated S1R flox

mouse will be a powerful tool to study cell-type-specific functions of the S1R in vivo.

AUTHOR CONTRIBUTIONS

WH conceptualized the project and designed experiments. WH and FK supervised the study. QL performed IHC, immunoblot, qPCR and confocal imaging. QG performed in-silico study, RiboTag immunoprecipitation and qPCR. L-PF performed MACS. AS performed AxioScan imaging. QL analysed data and generated figures. HY provided materials. WH and QL wrote and revised the manuscript with inputs from all other authors.

ACKNOWLEDGEMENT

We thank Daniel Schauenburg and colleagues for excellent animal husbandry and Frank Rhode for experimental assistance. This work was supported by grants from the Deutsche Forschungsgemeinschaft (HU 2614/1-1 (project ID: 462650276) to WH, Sino-German joint project KI 503/14-1 to WH and FK, SPP 1757, SFB 894 to FK); the Fritz Thyssen Foundation (10.21.1.021MN) and the Medical faculty of the University of Saarland (HOMFORexcellenz2016) to WH; the BMBF (EraNet-Neuron BrIE) and the European Commission (EC-H2020 FET ProAct Neurofibres) to FK; the National Natural Science Foundation of China (81761138048) to HY. QL was supported by a PhD student stipend from the Chinese Scholarship Council.

All experiments were conducted in compliance with the ARRIVE guidelines.

FUNDING INFORMATION

Deutsche Forschungsgemeinschaft DFG: HU 2614/1-1 (project ID: 462650276), Sino-German joint project KI 503/14, SPP 1757, SFB 894; Fritz Thyssen Foundation: 10.21.1.021MN; Medical faculty of the University of Saarland: HOMFORexcellenz2016; Bundesministerium für Bildung und Forschung (BMBF): EraNet-Neuron BrIE; European Commission: EC-H2020 FET ProAct Neurofibres; National Natural Science Foundation of China: 81761138048.

CONFLICT OF INTEREST

The authors declare no competing interests.

OPEN RESEARCH BADGES



This article has been awarded Open Materials Badge for making the components of the research methodology needed to reproduce the reported procedure and analysis publicly available at: <https://doi.org/10.1101/2022.06.08.494880>

DATA AVAILABILITY STATEMENT

House/custom-made materials will be shared upon reasonable request. This work was posted on bioRxiv as a preprint on June 12, 2022 (doi: <https://doi.org/10.1101/2022.06.08.494880>).

ORCID

Qing Liu <https://orcid.org/0000-0002-5245-1474>

Qilin Guo <https://orcid.org/0000-0002-7531-0818>

Li-Pao Fang <https://orcid.org/0000-0002-7973-9523>

Anja Scheller <https://orcid.org/0000-0001-8955-2634>

Frank Kirchhoff <https://orcid.org/0000-0002-2324-2761>

Wenhui Huang <https://orcid.org/0000-0001-9865-0375>

REFERENCES

- Abdullah, C. S., Aishwarya, R., Alam, S., Morshed, M., Remex, N. S., Nitu, S., Kolluru, G. K., Tralor, J., Miriyala, S., Panchatcharam, M., Hartman, B., King, J., Bhuiyan, M. A. N., Chandran, S., Matthew, D., Woolard, M. D., Yu, X., Goeders, N. E., Dominic, P., ... Bhuiyan, M. S. (2020). Methamphetamine induces cardiomyopathy by Sigmar1 inhibition-dependent impairment of mitochondrial dynamics and function. *Communications Biology*, 3(1), 682. <https://doi.org/10.1038/s42003-020-01408-z>
- Alonso, G., Phan, V., Guillemain, I., Saunier, M., Legrand, A., Anolo, M., & Maurice, T. (2000). Immunocytochemical localization of the sigma(1) receptor in the adult rat central nervous system. *Neuroscience*, 97(1), 155–170. [https://doi.org/10.1016/s0306-4522\(00\)00014-2](https://doi.org/10.1016/s0306-4522(00)00014-2)
- Brown, D., Lydon, J., McLaughlin, M., Stuart-Tilley, A., Tyszkowski, R., & Alper, S. (1996). Antigen retrieval in cryostat tissue sections and cultured cells by treatment with sodium dodecyl sulfate (SDS). *Histochemistry and Cell Biology*, 105(4), 261–267. <https://doi.org/10.1007/bf01463929>
- Consortium, T. M. (2020). A single-cell transcriptomic atlas characterizes ageing tissues in the mouse. *Nature*, 583(7817), 590–595. <https://doi.org/10.1038/s41586-020-2496-1>
- Couly, S., Gogvadze, N., Yasui, Y., Kimura, Y., Wang, S. M., Sharikadze, N., Wu, H. E., & Su, T. P. (2022). Knocking out sigma-1 receptors reveals diverse health problems. *Cellular and Molecular Neurobiology*, 42(3), 597–620. <https://doi.org/10.1007/s10571-020-00983-3>
- El-Brolosy, M. A., & Stainier, D. Y. R. (2017). Genetic compensation: A phenomenon in search of mechanisms. *PLoS Genetics*, 13(7), e1006780. <https://doi.org/10.1371/journal.pgen.1006780>
- Fang, L. P., Zhao, N., Caudal, L. C., Chang, H. F., Zhao, R., Lin, C. H., Hainz, N., Meier, C., Bettler, B., Huang, W., Scheller, A., Kirchhoff, F., & Bai, X. (2022). Impaired bidirectional communication between interneurons and oligodendrocyte precursor cells affects social cognitive behavior. *Nature Communications*, 13(1), 1394. <https://doi.org/10.1038/s41467-022-29020-1>
- Francardo, V., Bez, F., Wieloch, T., Nissbrandt, H., Ruscher, K., & Cenci, M. A. (2014). Pharmacological stimulation of sigma-1 receptors has neurorestorative effects in experimental parkinsonism. *Brain*, 137(Pt 7), 1998–2014. <https://doi.org/10.1093/brain/awu107>
- Goebbels, S., Bormuth, I., Bode, U., Hermanson, O., Schwab, M. H., & Nave, K. A. (2006). Genetic targeting of principal neurons in neocortex and hippocampus of NEX-Cre mice. *Genesis*, 44(12), 611–621. <https://doi.org/10.1002/dvg.20256>
- Hayashi, T., Lewis, A., Hayashi, E., Betenbaugh, M. J., & Su, T. P. (2011). Antigen retrieval to improve the immunocytochemistry detection of sigma-1 receptors and ER chaperones. *Histochemistry and Cell Biology*, 135(6), 627–637. <https://doi.org/10.1007/s00418-011-0811-5>
- Hayashi, T., & Su, T. P. (2004). Sigma-1 receptors at galactosylceramide-enriched lipid microdomains regulate oligodendrocyte differentiation. *Proceedings of the National Academy of Sciences of the United States of America*, 101(41), 14949–14954. <https://doi.org/10.1073/pnas.0402890101>
- Hayashi, T., & Su, T. P. (2007). Sigma-1 receptor chaperones at the ER-mitochondrion interface regulate Ca(2+) signaling and cell survival. *Cell*, 131(3), 596–610. <https://doi.org/10.1016/j.cell.2007.08.036>
- Hira, V. V. V., de Jong, A. L., Ferro, K., Khurshed, M., Molenaar, R. J., & Van Noorden, C. J. F. (2019). Comparison of different methodologies



- and cryostat versus paraffin sections for chromogenic immunohistochemistry. *Acta Histochemica*, 121(2), 125–134. <https://doi.org/10.1016/j.acthis.2018.10.011>
- Hirrlinger, P. G., Scheller, A., Braun, C., Quintela-Schneider, M., Fuss, B., Hirrlinger, J., & Kirchhoff, F. (2005). Expression of reef coral fluorescent proteins in the central nervous system of transgenic mice. *Molecular and Cellular Neurosciences*, 30(3), 291–303. <https://doi.org/10.1016/j.mcn.2005.08.011>
- Huang, W., Bai, X., Meyer, E., & Scheller, A. (2020). Acute brain injuries trigger microglia as an additional source of the proteoglycan NG2. *Acta Neuropathologica Communications*, 8(1), 146. <https://doi.org/10.1186/s40478-020-01016-2>
- Huang, W., Guo, Q., Bai, X., Scheller, A., & Kirchhoff, F. (2019). Early embryonic NG2 glia are exclusively gliogenic and do not generate neurons in the brain. *Glia*, 67, 1094–1103. <https://doi.org/10.1002/glia.23590>
- Huang, W., Zhao, N., Bai, X., Karram, K., Trotter, J., Goebbels, S., Scheller, A., & Kirchhoff, F. (2014). Novel NG2-CreERT2 knock-in mice demonstrate heterogeneous differentiation potential of NG2 glia during development. *Glia*, 62(6), 896–913. <https://doi.org/10.1002/glia.22648>
- Ishii, A., Fyffe-Maricich, S. L., Furusho, M., Miller, R. H., & Bansal, R. (2012). ERK1/ERK2 MAPK signaling is required to increase myelin thickness independent of oligodendrocyte differentiation and initiation of myelination. *The Journal of Neuroscience*, 32(26), 8855–8864. <https://doi.org/10.1523/jneurosci.0137-12.2012>
- Jahn, O., Tenzer, S., & Werner, H. B. (2009). Myelin proteomics: molecular anatomy of an insulating sheath. *Molecular Neurobiology*, 40(1), 55–72. <https://doi.org/10.1007/s12035-009-8071-2>
- Kopanchuk, S., Vavers, E., Veikinska, S., Ligi, K., Zvejniece, L., Dambrova, M., & Rincken, A. (2022). Intracellular dynamics of the Sigma-1 receptor observed with super-resolution imaging microscopy. *PLoS One*, 17(5), e0268563. <https://doi.org/10.1371/journal.pone.0268563>
- Lafamme, C., McKeever, P. M., Kumar, R., Schwartz, J., Kolahdouzan, M., Chen, C. X., You, Z., Benaliouad, F., Gileadi, O., McBride, H. M., Durcan, T. M., Edwards, L. M., Healy, L. M., Robertson, J., & McPherson, P. S. (2019). Implementation of an antibody characterization procedure and application to the major ALS/FTD disease gene C9ORF72. *eLife*, 8, e48363. <https://doi.org/10.7554/eLife.48363>
- Lee, P. T., Liévens, J. C., Wang, S. M., Chuang, J. Y., Khalil, B., Wu, H. E., Maurice, T., & Su, T. P. (2020). Sigma-1 receptor chaperones rescue nucleocytoplasmic transport deficit seen in cellular and Drosophila ALS/FTD models. *Nature Communications*, 11(1), 5580. <https://doi.org/10.1038/s41467-020-19396-3>
- Mavlyutov, T. A., Duellman, T., Kim, H. T., Epstein, M. L., Leese, C., Davletov, B. A., & Yang, J. (2016). Sigma-1 receptor expression in the dorsal root ganglion: Reexamination using a highly specific antibody. *Neuroscience*, 331, 148–157. <https://doi.org/10.1016/j.neuroscience.2016.06.030>
- Mavlyutov, T. A., Epstein, M. L., Andersen, K. A., Ziskind-Conhaim, L., & Ruoho, A. E. (2010). The sigma-1 receptor is enriched in post-synaptic sites of C-terminals in mouse motoneurons. An anatomical and behavioral study. *Neuroscience*, 167(2), 247–255. <https://doi.org/10.1016/j.neuroscience.2010.02.022>
- Moreno, E., Moreno-Delgado, D., Navarro, G., Hoffmann, H. M., Fuentes, S., Rosell-Vilar, S., Gasperini, P., Rodríguez-Ruiz, M., Medrano, M., Mallol, J., Cortés, A., Casadó, V., Lluís, C., Ferré, S., Ortiz, J., Canela, E., & McCormick, P. J. (2014). Cocaine disrupts histamine H3 receptor modulation of dopamine D1 receptor signaling: σ 1-D1-H3 receptor complexes as key targets for reducing cocaine's effects. *The Journal of Neuroscience*, 34(10), 3545–3558. <https://doi.org/10.1523/jneurosci.4147-13.2014>
- Mori, T., Tanaka, K., Buffo, A., Wurst, W., Kuhn, R., & Gotz, M. (2006). Inducible gene deletion in astroglia and radial glia—A valuable tool for functional and lineage analysis. *Glia*, 54(1), 21–34. <https://doi.org/10.1002/glia.20350>
- Nakamura, Y., Dryanovski, D. I., Kimura, Y., Jackson, S. N., Woods, A. S., Yasui, Y., Tsai, S. Y., Patel, S., Covey, D. P., Su, T. P., & Lupica, C. R. (2019). Cocaine-induced endocannabinoid signaling mediated by sigma-1 receptors and extracellular vesicle secretion. *eLife*, 8, e47209. <https://doi.org/10.7554/eLife.47209>
- Palacios, G., Muro, A., Vela, J. M., Molina-Holgado, E., Guitart, X., O valle, S., & Zamanillo, D. (2003). Immunohistochemical localization of the sigma1-receptor in oligodendrocytes in the rat central nervous system. *Brain Research*, 961(1), 92–99. [https://doi.org/10.1016/s0006-8993\(02\)03892-1](https://doi.org/10.1016/s0006-8993(02)03892-1)
- Ruscher, K., Shamloo, M., Rickhag, M., Ladunga, I., Soriano, L., Gisselsson, L., Torsson, H., Ruslim-Litrus, L., Oksenberg, D., Urfer, R., Johansson, B. B., Nikolich, K., & Wieloch, T. (2011). The sigma-1 receptor enhances brain plasticity and functional recovery after experimental stroke. *Brain*, 134(Pt 3), 732–746. <https://doi.org/10.1093/brain/awq367>
- Saab, A. S., Tzvetavona, I. D., Trevisiol, A., Baltan, S., Dibaj, P., Kusch, K., Möbius, W., Goetze, B., Jahn, H. M., Huang, W., Steffens, H., Schomburg, E. D., Pérez-Samartín, A., Pérez-Cerdá, F., Bakhtiari, D., Matute, C., Löwel, S., Griesinger, C., Hirrlinger, J., & Nave, K. A. (2016). Oligodendroglial NMDA receptors regulate glucose import and axonal energy metabolism. *Neuron*, 91(1), 119–132. <https://doi.org/10.1016/j.neuron.2016.05.016>
- Sałaciak, K., & Pytka, K. (2022). Revisiting the sigma-1 receptor as a biological target to treat affective and cognitive disorders. *Neuroscience and Biobehavioral Reviews*, 132, 1114–1136. <https://doi.org/10.1016/j.neubiorev.2021.10.037>
- Sanz, E., Yang, L., Su, T., Morris, D. R., McKnight, G. S., & Amieux, P. S. (2009). Cell-type-specific isolation of ribosome-associated mRNA from complex tissues. *Proceedings of the National Academy of Sciences of the United States of America*, 106(33), 13939–13944. <https://doi.org/10.1073/pnas.0907143106>
- Schmidt, H. R., & Kruse, A. C. (2019). The molecular function of σ receptors: past, present, and future. *Trends in Pharmacological Sciences*, 40(9), 636–654. <https://doi.org/10.1016/j.tips.2019.07.006>
- Shi, S. R., Cote, R. J., & Taylor, C. R. (1997). Antigen retrieval immunohistochemistry: past, present, and future. *The Journal of Histochemistry and Cytochemistry*, 45(3), 327–343. <https://doi.org/10.1177/002215549704500301>
- Stuart, T., Butler, A., Hoffman, P., Hafemeister, C., Papalexi, E., Mauck, W. M., Hao, Y., Stoekius, M., Smibert, P., & Satija, R. (2019). Comprehensive integration of single-cell data. *Cell*, 177(7), 1888–1902.e1821. <https://doi.org/10.1016/j.cell.2019.05.031>
- Su, T. P., Su, T. C., Nakamura, Y., & Tsai, S. Y. (2016). The sigma-1 receptor as a pluripotent modulator in living systems. *Trends in Pharmacological Sciences*, 37(4), 262–278. <https://doi.org/10.1016/j.tips.2016.01.003>
- Wang, R. H., Li, C., & Deng, C. X. (2010). Liver steatosis and increased ChREBP expression in mice carrying a liver specific SIRT1 null mutation under a normal feeding condition. *International Journal of Biological Sciences*, 6(7), 682–690. <https://doi.org/10.7150/ijbs.6.682>
- Weruaga, E., Alonso, J. R., Porteros, A., Crespo, C., Arévalo, R., Briñón, J. G., Valasco, A., & Aijón, J. (1998). Nonspecific labeling of myelin with secondary antisera and high concentrations of Triton X-100. *The Journal of Histochemistry and Cytochemistry*, 46(1), 109–118. <https://doi.org/10.1177/002215549804600114>
- Wilson, D. M., & Bianchi, C. (1999). Improved immunodetection of nuclear antigens after sodium dodecyl sulfate treatment of formaldehyde-fixed cells. *The Journal of Histochemistry and Cytochemistry*, 47(8), 1095–1100. <https://doi.org/10.1177/002215549904700814>
- Ximerakis, M., Lipnick, S. L., Innes, B. T., Simmons, S. K., Adiconis, X., Dionne, D., Mayweather, B. A., Nguyen, L., Nizioletk, Z., Ozek, C., Butty, V. L., Isserlin, R., Buchanan, S. M., Levine, S. S., Regev, A., Bader, G. D., Levin, J. Z., & Rubin, L. L. (2019). Single-cell transcriptomic profiling of the aging mouse brain. *Nature Neuroscience*, 22(10), 1696. <https://doi.org/10.1038/s41593-019-0491-3>



- Yang, H., Shen, H., Li, J., Stanford, K. I., & Guo, L. W. (2020). Sigma-1 receptor ablation impedes adipocyte-like differentiation of mouse embryonic fibroblasts. *Cellular Signalling*, 75, 109732. <https://doi.org/10.1016/j.cellsig.2020.109732>
- Yona, S., Kim, K. W., Wolf, Y., Mildner, A., Varol, D., Breker, M., Strauss-Ayali, D., Viukov, S., Guilliams, M., Misharin, A., Hume, D. A., Perlman, P., Malissen, B., Zelzer, E., & Jung, S. (2013). Fate mapping reveals origins and dynamics of monocytes and tissue macrophages under homeostasis. *Immunity*, 38(1), 79–91. <https://doi.org/10.1016/j.immuni.2012.12.001>
- Zhang, Y., Chen, K., Sloan, S., Bennett, M., Scholze, A., O'Keefe, S., Phatnani, H. P., Guarnieri, P., Caneda, C., Ruderisch, N., Deng, S., Liddelow, S. A., Zhang, C., Daneman, R., Maniatis, T., Barres, B. A., & Wu, J. (2014). An RNA-sequencing transcriptome and splicing database of glia, neurons, and vascular cells of the cerebral cortex. *Journal of Neuroscience*, 34(36), 11929–11947. <https://doi.org/10.1523/JNEUROSCI.1860-14.2014>
- Zhemkov, V., Ditlev, J. A., Lee, W. R., Wilson, M., Liou, J., Rosen, M. K., & Bezprozvanny, I. (2021). The role of sigma 1 receptor in organization

of endoplasmic reticulum signaling microdomains. *eLife*, 10, e65192. <https://doi.org/10.7554/eLife.65192>

SUPPORTING INFORMATION

Additional supporting information can be found online in the Supporting Information section at the end of this article.

How to cite this article: Liu, Q., Guo, Q., Fang, L.-P., Yao, H., Scheller, A., Kirchhoff, F., & Huang, W. (2023). Specific detection and deletion of the sigma-1 receptor widely expressed in neurons and glial cells *in vivo*. *Journal of Neurochemistry*, 164, 764–785. <https://doi.org/10.1111/jnc.15693>